

Neutron capture and total cross sections of ^{127}I and ^{129}I

G. Noguere and O. Bouland

CEA/Cadarache, F-13108 Saint Paul lez Durance, France

A. Brusegan,* P. Schillebeeckx, and P. Siegler

EC-JRC-IRMM, B-2440 Geel, Belgium

A. Leprêtre and N. Herault

CEA Saclay, F-91191 Gif sur Yvette, France

G. Rudolf

Ires Strasbourg/IN2P3, F-67037 Strasbourg, France

(Received 10 January 2005; revised manuscript received 7 June 2006; published 6 November 2006)

High-resolution transmission and capture time-of-flight measurements of ^{127}I and ^{129}I have been carried out at the 150 MeV pulsed neutron source at the Geel electron linear accelerator (GELINA) facility of the Institute for Reference Materials and Measurements. Below 10 keV, the individual resonances were analyzed with the Reich-Moore approximation of the R -matrix theory. The resonance parameters (energy and partial widths) and the potential scattering length R_0' were determined using the resonance shape analysis technique. Within the 3.5–100 keV neutron energy range, the capture and total cross sections were interpreted in terms of average resonance parameters with the Hauser-Feshbach formalism with width fluctuations. This work has delivered a consistent set of $^{127,129}\text{I}$ s - and p -wave average resonance parameters (neutron strength function S_l , mean level spacing D_l , and average radiation width $\langle\Gamma\gamma_l\rangle$).

DOI: [10.1103/PhysRevC.74.054602](https://doi.org/10.1103/PhysRevC.74.054602)

PACS number(s): 25.40.Ny, 25.60.Dz, 25.70.Gh, 25.70.Ef

I. INTRODUCTION

The main objective of partitioning and transmutation (P-T) studies is to develop the technology to efficiently transmute minor actinides of high toxicity such as ^{237}Np , $^{241,243}\text{Am}$, and $^{244,245}\text{Cm}$, and some long-lived fission products such as ^{99}Tc , ^{129}I , and ^{135}Cs using reactors (fast or thermal) or hybrid systems.

With 400 kg of ^{129}I produced yearly in European reactors and a very long β^- half-life of 1.57×10^7 years, iodine requires disposal strategies that will isolate this isotope from the environment for a very long period of time. However, iodine is considered difficult to isolate as it may migrate into the groundwater and move throughout the ecosystem. ^{129}I is potentially a good candidate for P-T applications: after one single neutron capture, ^{129}I transmutes in ^{130}I and decays to the noble gas ^{130}Xe with a 12.36 h half-life.

The capture cross section of the radioactive iodine ^{129}I was measured more than 20 years ago at the Oak Ridge electron linear accelerator (ORELA) by Macklin [1]. Improvements of the capture cross section within the thermal and epithermal energy ranges are needed to evaluate the transmutation potential of ^{129}I in reactor configuration. For that purpose, time-of-flight (TOF) measurements covering the energy range from 0.5 eV to 100 keV have been carried out at the 150 MeV pulsed neutron source at the Geel electron linear accelerator (GELINA) of the Institute for Reference Materials and Measurements (IRMM) in Geel, Belgium. Two types of experiments have been

performed—capture and transmission—related, respectively, to neutron capture and total cross sections. Since the PbI_2 samples used in this work contain natural and radioactive iodine, extensive measurements of ^{127}I have been carried out under the same experimental conditions as for ^{129}I . Preliminary and intermediate results can be found in Refs. [2,3].

This paper focuses on the experimental method and on the data analysis used to determine the ^{127}I and ^{129}I total and capture cross sections. For the analysis, we have distinguished the resolved and unresolved resonance range (RRR and URR). A consistent description of these two regions has been assessed by means of an appropriate statistical interpretation of the individual Reich-Moore resonance parameters into Hauser-Feshbach average parameters.

II. SAMPLE PREPARATION

Although the ideal target material would have been elemental iodine, this choice was rapidly ruled out in view of the radiological hazard, volatility, and reactivity of I_2 . A PbI_2 compound was considered a reasonable compromise, with no lead resonances in the resolved resonance energy range of the iodine isotopes. Besides, lead has a low capture cross section, and pressed PbI_2 is mechanically more stable. The characteristics of the samples are given in Table I.

Four samples containing commercial $\text{Pb}^{127}\text{I}_2$ powder were prepared at the IRMM. Thin samples were designed to study the broad resonances at 20.4, 31.2, 37.6, and 45.3 eV. Otherwise, broad resonances with a high peak cross section value are “black” in transmission or “saturated” in capture. For

*Deceased.

TABLE I. Sample characteristics.

Experiment	Sample	Diameter (mm)	^{127}I thickness (at/b)	^{129}I thickness (at/b)
^{127}I transmission	Thin PbI_2	55	$(7.09 \pm 0.10) \times 10^{-4}$	
	LiI	100	$(9.45 \pm 0.11) \times 10^{-4}$	
^{127}I capture	Thick PbI_2	55	$(2.38 \pm 0.04) \times 10^{-2}$	
	Thin PbI_2	80	$(9.48 \pm 0.22) \times 10^{-4}$	
^{129}I transmission	Thick PbI_2	80	$(4.76 \pm 0.09) \times 10^{-3}$	
	Thin PbI_2	55	$(1.47 \pm 0.04) \times 10^{-4}$	$(7.09 \pm 0.17) \times 10^{-4}$
^{129}I capture	Thick PbI_2	55	$(1.46 \pm 0.04) \times 10^{-3}$	$(7.08 \pm 0.18) \times 10^{-3}$
	Thin PbI_2	80	$(1.56 \pm 0.05) \times 10^{-4}$	$(7.56 \pm 0.18) \times 10^{-4}$
	Thick PbI_2	80	$(7.90 \pm 0.23) \times 10^{-4}$	$(3.81 \pm 0.09) \times 10^{-3}$

technical reasons, it was necessary to increase the physical thickness of the so-called thin samples by using a low structureless cross section diluent powder. In this work, the $\text{Pb}^{127}\text{I}_2$ powder was mixed with a large amount of sulfur (about 1 g/cm²). However, the homogeneity of the mixture was unknown. Parallel independent measurements were performed with a liquid sample of Li^{127}I , especially designed to study the low neutron energy of the ^{127}I total cross section. The use of ionic compounds dissolved in water enabled us to prepare very thin homogeneous samples of 1 mm thick.

For ^{129}I , the starting material was 210 l of waste solution provided by the French fuel reprocessing facility of La Hague. The solution, containing 1.3 g/l of iodine, had been made alkaline ($\text{pH} = 14$) using Na_2CO_3 in order to keep the iodine in solution. Though well documented, the chemistry of iodine remains complex. The nature of species formed during a reaction is not always predictable. Indeed, numerous oxidation states are possible, and iodine may also form compounds with itself, oxygen, and other elements. The procedure for the separation of the iodine from the mother solution was developed and optimized at the IRMM [4]. This procedure involved three steps: (1) acidification and oxidation of iodide (I^-) to iodine (I_2) with nitric acid and extraction of the I_2 into chloroform (CHCl_3); (2) reduction of iodine to iodide with sodium sulfite (Na_2SO_3) and extraction back into an aqueous phase; and (3) precipitation of iodine as PbI_2 by the addition of $\text{Pb}(\text{NO}_3)_2$. The total quantity of ^{129}I extracted was about 140 g. The samples were canned by compaction of the powder into cylindrical aluminum containers of different sizes.

The preparation and mass determination of the sample is a crucial step in the experimental procedure. The characterization of the radioactive PbI_2 samples was done by activation measurements, neutron resonance capture analysis (NRCA), inductively coupled plasma mass spectrometry (ICP-MS), and conventional chemical methods. Our radioactive PbI_2 samples have a complex elemental composition involving natural and radioactive iodine ($3.36 \pm 0.08\%$ and $16.49 \pm 0.40\%$), non-negligible amount of natural lead ($53.5 \pm 3.0\%$), sulfur ($6.2 \pm 0.4\%$), sodium ($0.75 \pm 0.04\%$), hydrogen (0.09%), oxygen ($14.5 \pm 1.5\%$), and nitrogen ($1.2 \pm 0.4\%$). The global accuracy of the ^{127}I and ^{129}I mass fractions is close to 2.5%.

III. EXPERIMENTAL TECHNIQUES

A. The GELINA facility

Experiments on iodine were performed at the Geel electron linear accelerator (GELINA) of the Institute for Reference Materials and Measurements. The measurements are based on the time-of-flight method. Detected events are correlated to the neutron energy by measuring the time elapsed since the generation of the neutron burst. The neutron source of the GELINA facility consists of a mercury-cooled uranium target. Neutrons are produced in a two-step process. Intense bremsstrahlung is generated after slowing down of fast electrons in the target. Short bursts of fast neutrons are then produced via (γ, n) reactions and to a lesser extent via (γ, f) reactions. To enhance the neutron spectrum intensity below a few hundred keV, two 36 mm water slabs in a beryllium canning are placed just above and below the target. The neutrons emitted from the target-moderator assembly are led to the experimental areas along neutron flight paths. The transmission and capture experimental areas are shown in Fig. 1. Detailed descriptions of the experimental techniques are given elsewhere [5,6].

B. Measuring sequences

Capture and transmission experiments are divided into several sequences of sample changer positions. The sample changers are monitored by the acquisition systems and expose different filters to the neutron beam in a repetitive way. As the experiments took several weeks, the sequence had to be short enough to reduce the systematic uncertainties resulting from a possible instability of the accelerator and from any variations of the sample temperature. In TOF measurements, two types of filters can be distinguished. Permanent antioverlap filters eliminate the slowest neutrons of each burst, while black resonance filters are used for determining the time-dependent background.

In our transmission and capture measurements, adequate thicknesses of W, Ge, Mo, Co, Na, S, and Bi were placed in the neutron beamline in order to absorb nearly all neutrons in a given energy region. In that way, any count rate observed below a black resonance could be attributed to the background.

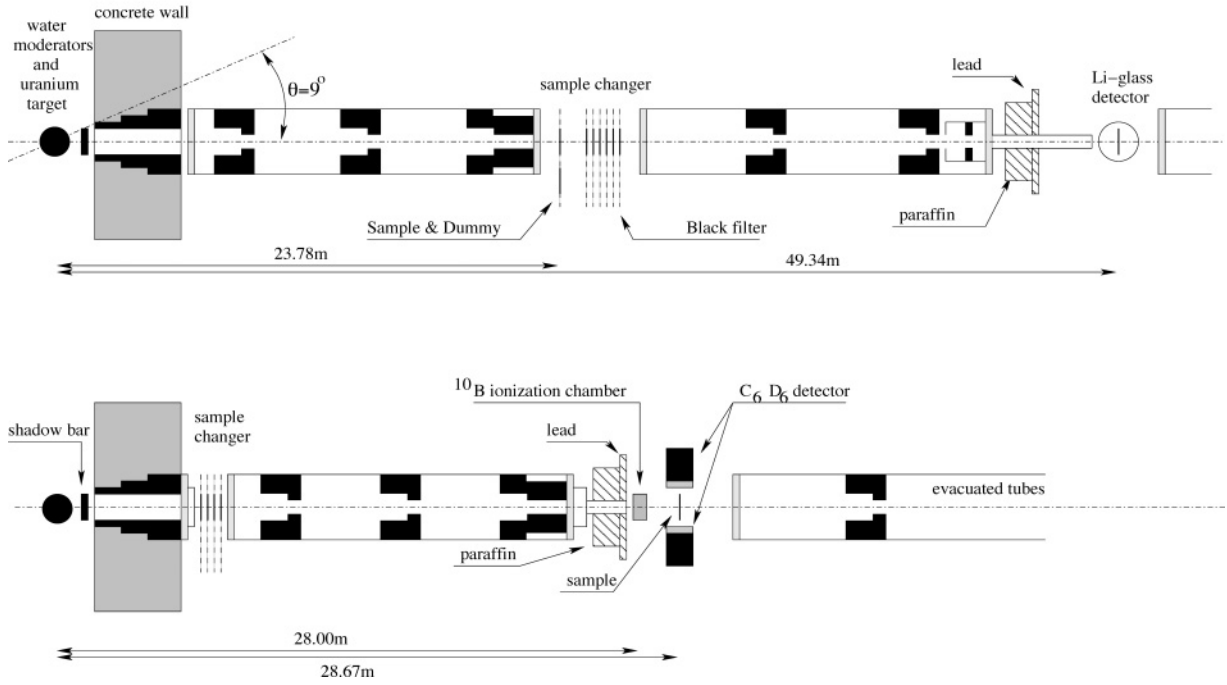


FIG. 1. Schemes of the transmission and capture flight paths.

The energy-dependent background was interpolated between the different black resonance regions with a simple function of time.

Antioverlap filters have a different goal. Without them, slow neutrons from a given burst get mixed up with neutrons from the next burst. To prevent overlap, boron or cadmium filters are placed in the neutron beamline. At a 800 Hz repetition rate, the perfect $1/\nu$ behavior of the boron total cross section is suitable for investigating a large neutron energy range. At a 100 Hz repetition rate, we take advantage of the so-called Cd cutoff at 0.2 eV to study the energy range below 10 eV.

C. Transmission experiments

In transmission measurements, the neutrons cross a filter setup and the sample/dummy at a distance of 23.7 m. Neutrons are detected at 49.34 m with a 1/4 in. thick Li glass (NE912) viewed by a 5 in. EMI 9823 KQB photomultiplier. The latter is placed at a right angle to the neutron beam axis. The neutron beam diameter is 45 mm.

The transmission experiment consists of measuring the attenuation of the incident neutron beam going through a sample of thickness n at/b. The transmission factor $T(E)$ is then expressed as the ratio of the transmitted neutron flux $\phi_{\text{out}}(E)$ and the incident flux $\phi_{\text{in}}(E)$:

$$T(E) \propto \frac{\phi_{\text{in}}(E)}{\phi_{\text{out}}(E)}. \quad (1)$$

Experimentally, this transmission factor is obtained from the ratio of a sample-in measurement $C_{\text{in}}(E)$ and a sample-out measurement $C_{\text{out}}(E)$, both corrected for dead time [$a_{\text{in}}(E)$ and $a_{\text{out}}(E)$] and background contributions [$B_{\text{in}}(E)$ and $B_{\text{out}}(E)$], that is,

$$T(E) = N_T \frac{a_{\text{in}}(E)C_{\text{in}}(E) - B_{\text{in}}(E)}{a_{\text{out}}(E)C_{\text{out}}(E) - B_{\text{out}}(E)}, \quad (2)$$

in which N_T stands for the normalization factor. The latter accounts for the differences in integrated intensities of the incident neutron beam during the sample-in and sample-out cycles. N_T was estimated by monitoring the neutron flux using four BF_3 tubes (TGM25) located in the armored concrete roof above the uranium target of GELINA. These detectors are called central monitors (CMs). They give an accurate normalization of the transmission data with a maximum dispersion of about 0.5%. The experimental dead time per event of $1.42 \mu\text{s}$ was continuously monitored during the measurement. Corrections of less than 2.4% and 3.5% for the data taken at 100 and 800 Hz, respectively, were applied below 1 keV. The background was determined in the minima of specific resonances with the black resonance technique, as explained in Sec. III B. At 1 keV, the background contribution was of the order of 4%.

D. Capture experiments

For the capture experiment, the sample is located 28.67 m from the neutron source. The experimental setup consists of three detectors. The neutron flux is measured with a ^{10}B

ionization chamber, while capture γ rays emitted from the sample are detected by two C_6D_6 liquid scintillators (NE230) placed at 90° with respect to the beam axis. A series of collimators results in a neutron beam with a diameter of 75 mm.

In this work, the neutron capture cross section is measured by detecting the prompt γ rays emitted when the compound nucleus deexcites to its ground state. In practice, we measure a capture yield $Y(E)$ defined as the number of capture events $N_c(E)$ per incident neutron $\phi(E)$. The essential requirement for a radiative neutron capture detector is that its efficiency is independent of the capture γ -ray spectrum. This result can be achieved by using a total energy detector which has the property of making the probability of detecting a capture event proportional to the excitation energy E^* of the compound nucleus. In the present work, this condition is realized by weighing the pulse amplitude response of small deuterate benzene C_6D_6 liquid scintillators with a weighting function W . The latter was measured at the IRMM by Corvi [7]. The experimental capture yield $Y(E)$ is then expressed as

$$Y(E) = N_Y \frac{N_c(E)}{\phi(E)} = \frac{N_Y a(E) \sum_I C_\gamma(I, E) W(I) - B_\gamma(E)}{E^* a(E) C_F(E) - B_F(E)} \sigma_{n,\alpha}^B(E), \quad (3)$$

in which N_Y represents the normalization factor, $a(E)$ is the dead time correction, $C_\gamma(I, E)$ is the count rate observed at a given pulse height energy, $C_F(E)$ stands for the count rate delivered by the boron chamber, $\sigma_{n,\alpha}^B(E)$ is the $^{10}B(n, \alpha)$ cross section, $B_\gamma(E)$ and $B_F(E)$ are the background contributions, and $W(I)$ is the weighting function expressed as a function of the γ -ray energy I .

The normalization N_Y was achieved by analyzing simultaneously the capture and transmission data. This technique led to a normalization accuracy of about 3%. The time-dependent background in the neutron flux spectrum was estimated with the black resonance technique. At 1 keV, the contribution of the background was less than 1.3%. For the C_6D_6 , we determined the shape of the background together with the resonance parameters. The background contribution reaches 4% near 1 keV. In our analysis, the prompt component of the time-dependent background was disregarded. The former originates from secondary neutrons produced in reactions such as (n, n) , (n, n') , or $(n, 2n)$ and subsequently captured in the detector environment. This effect acquires a significant importance for structural materials where $\Gamma_n/\Gamma_\gamma > 10^3$.

E. Data reduction

The data reduction procedure is divided into several sequences of operation. Bastian wrote a set of commands for neutron data reduction called AGS [8]. The AGS system concerns basic operations such as spectrum addition or division, dead time correction, nonlinear fitting, and several other involved operations, preserving all the steps in a single file with full uncertainty propagation. A large number of data sets covering the energy range from 0.5 eV to 100 keV was obtained, together with experimental covariance matrices.

The last step of the data reduction procedure consists of producing experimental average cross sections that are used for analyzing the unresolved resonance range in terms of average resonance parameters. To deduce a set of average parameters from experimental capture and transmission data, one has to account for the fluctuations of the cross section and the multiple scattering effects. For that purpose, we used the Monte Carlo code SESH [9], which was especially written for the calculation of sample thickness corrections to resonance-averaged transmission and capture data. The program simulates multiple collision events and calculates the corrections for cylindrical samples. For each neutron energy, it generates a resonance environment by sampling resonance spacing and partial widths from the Wigner level spacing [10] and Porter-Thomas reduced neutron width [11] distributions. The Doppler-broadened total, capture, and scattering cross sections are then computed from the sampled resonance parameters in the single-level Breit-Wigner (SLBW) approximation [12]. The final results given by the SESH code consist of two correction factors C_T and C_Y . The total $\langle\sigma_t(E)\rangle$ and capture $\langle\sigma_\gamma(E)\rangle$ pointwise cross sections are then deduced as follows:

$$\langle\sigma_t(E)\rangle = -\frac{1}{n} \ln \frac{\langle T(E)\rangle}{C_T(E)} - \sum_i \frac{n_i}{n} \langle\sigma_{t,i}(E)\rangle, \quad (4)$$

$$\langle\sigma_\gamma(E)\rangle = \frac{1}{n} \frac{\langle Y(E)\rangle}{C_Y(E)} - \sum_i \frac{n_i}{n} \langle\sigma_{\gamma,i}(E)\rangle \varepsilon_i, \quad (5)$$

in which $\langle T(E)\rangle$ and $\langle Y(E)\rangle$ stand for the experimental transmission [Eq. (2)] and capture yield [Eq. (3)] averaged over a suitable energy mesh, n is the sample thickness of the isotope under investigation, and i labels the contributions of the other isotopes within the sample (n_i is the thickness in atoms per barn and ε_i stands for the capture detection efficiency). For our capture setup, ε_i is expressed as the ratio of the excitation energies of isotope i to the isotope under investigation (E_i^*/E^*).

IV. THE RESOLVED RESONANCE RANGE

The cross sections determined in this work result from the analysis of 18 TOF measurements. The resolved resonance range (RRR) was analyzed up to 10 keV with the shape analysis programs REFIT [13] and SAMMY [14]. Below 5 keV, the resonance parameters were extracted with a simultaneous analysis of the transmission and capture measurements. Within the 5–10 keV energy range, the neutron width values and resonance energies were determined with the transmission data alone.

A. Resonance shape analysis

The REFIT [13] and SAMMY [14] codes adjust nuclear parameters so that the theoretical curve agrees with the observed data within the limit of the uncertainties. In the RRR, the nuclear parameters are the energy E_0 , the neutron and radiation widths Γ_n, Γ_γ , the total angular momentum J , the orbital momentum l , and the effective radii R' . The

theoretical cross sections are generated with the Reich-Moore approximation of the R -matrix formalism [15] and Doppler broadened using the ideal free gas model with a given effective temperature as suggested in Lamb's theory [16]. The theoretical transmission $T_{\text{th}}(E)$ and capture yield $Y_{\text{th}}(E)$ are calculated as

$$T_{\text{th}}(E) = \exp \left[- \sum_i n_i \sigma_{t,i}(E) \right], \quad (6)$$

$$Y_{\text{th}}(E) = \mu(E) [1 - T_{\text{th}}(E)] \frac{\sum_i n_i \sigma_{\gamma,i}(E)}{\sum_i n_i \sigma_{t,i}(E)}, \quad (7)$$

in which i labels the contribution of the various isotopes contained in the sample, $\mu(E)$ represents the self-shielding and multiple scattering effects, $\sigma_t(E)$ and $\sigma_{\gamma}(E)$ stand for the total and capture Doppler-broadened cross sections.

It is not possible to proceed to a direct comparison of the cross sections generated via the Reich-Moore formalism with the capture and transmission data. To confront experiments with the theory, expressions (6) and (7) must be broadened with the experimental resolution function $R(E)$ of the GELINA facility. The theoretical curves are calculated as

$$T(E) = \int_0^{\infty} R(E, E') T_{\text{th}}(E') dE', \quad (8)$$

$$Y(E) = \int_0^{\infty} R(E, E') Y_{\text{th}}(E') dE'. \quad (9)$$

The description of the experimental resolution function of the GELINA facility and its impact on the resonance parameters were poorly documented. During this work, its analytic treatment has been significantly improved with Monte Carlo simulations carried out by Coceva [17]. The systematic error affecting the area of isolated resonances was reduced to 3% [18].

B. External levels

The thermal capture and total cross sections are essential ingredients in the determination of the contribution of the external levels and of the potential scattering. The thermal cross section is the resulting cross section of the tails of all resonances including negative resonances corresponding to levels below the neutron binding energy. Various *ad hoc* approaches exist to describe their contributions. A convenient approximation involves using broad negative resonances [19]. Their resonance parameters and the effective potential scattering length R'_0 are determined simultaneously by including in the fitting procedure experimental thermal cross section values with transmission and capture data.

^{127}I thermal capture cross sections reported in the literature are listed in Table II. A significant discrepancy of about 19.2% exists between the two recent measurements carried out at the Rikkyo University research reactor by Katoh [31] and obtained at the 10 MW Budapest research reactor by Belgya [32]. Consequently, we decided to determine external levels and R'_0 values of ^{127}I with the weighed mean value of the thermal capture cross sections given in Table II. Starting

TABLE II. ^{127}I thermal capture ($\sigma_{\gamma}^{\text{th}}$) and total (σ_t^{th}) cross sections. The thermal value reported by Grimeland is not included in the weighed mean value used in this work.

Author	Ref.	Year	σ_t^{th} (barns)
Dunning	[20]	1935	9.4
Rainwater	[21]	1947	10.3
Author	Ref.	Year	$\sigma_{\gamma}^{\text{th}}$ (barns)
Seren	[22]	1947	6.65 ± 1.3
Pomerance	[23]	1951	6.3 ± 0.32
Grimeland	[24]	1952	5.03
Tattersall	[25]	1960	6.6 ± 0.3
Meadows	[26]	1961	6.22 ± 0.15
Jozefowicz	[27]	1963	5.84 ± 0.2
Robertson	[28]	1965	6.17 ± 0.2
Ryves	[29]	1970	6.12 ± 0.12
Friedmann	[30]	1983	4.7 ± 0.2
Katoh	[31]	1999	6.4 ± 0.29
Belgya	[32]	2004	5.4 ± 0.1
weighed mean value (used in this work)			5.80 ± 0.05

with the prior ^{127}I parameters recommended in the Japanese Evaluated Nuclear Data File JENDL-3.3 and with a channel radius $a_c = 6.801$ fm, we obtained the following posterior values for the parameters of the negative resonances:

$$\begin{cases} E_-(J^{\pi} = 2^+) = -54.2 \pm 0.1 \text{ eV}, \\ \Gamma_{\gamma}(J^{\pi} = 2^+) = 99.8 \pm 1.0 \text{ meV}, \\ \Gamma_n(J^{\pi} = 2^+) = 116.3 \pm 1.1 \text{ meV}, \end{cases}$$

$$\begin{cases} E_-(J^{\pi} = 3^+) = -43.3 \pm 0.1 \text{ eV}, \\ \Gamma_{\gamma}(J^{\pi} = 3^+) = 98.3 \pm 0.9 \text{ meV}, \\ \Gamma_n(J^{\pi} = 3^+) = 111.8 \pm 1.0 \text{ meV}, \end{cases}$$

And for the s -wave effective radius,

$$R'_0 = 5.5 \pm 0.1 \text{ fm}.$$

The accuracies quoted on the resonance parameters were determined with the SAMMY code. The uncertainty on R'_0 takes into account the statistical uncertainty, the accuracy of the normalization factor and of the sample thickness. Contributions at low neutron energies of the external levels to ^{127}I cross sections are shown in the upper part of Fig. 2, and are compared with experimental results reported in the literature.

For iodine 129, five earlier works report thermal capture cross section measurements (Table III). Among them, Roy, Friedmann, and Nakamura used the activation technique with a near-core reactor based thermal spectrum, whereas Block and Pattenden measured the total cross section at the ORNL fast chopper time-of-flight neutron spectrometer. The measurements based on the activation technique yield discrepant values. The result provided by Roy is questionable because the existence of the isomeric state ^{130m}I (9.2 min) was established later in 1966 [37]. The radiative capture of neutrons is then complicated by the activation of the metastable state

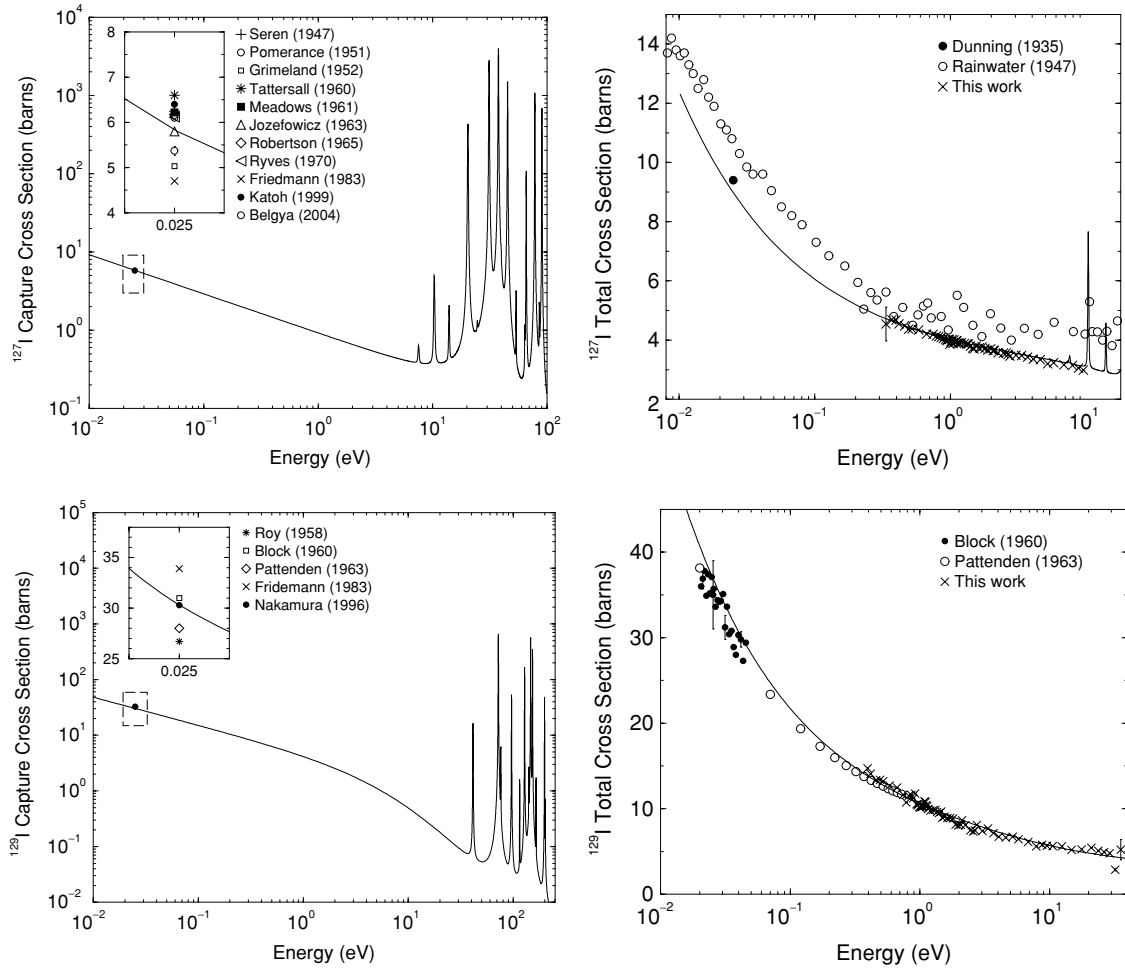


FIG. 2. Solid curves represent the Reich-Moore description of the low neutron energy range of the $^{127,129}\text{I}$ capture and total cross sections. Thermal values reported in the literature are given in Tables II and III.

of ^{130}I . The in-beam technique used by Block and Pattenden is insensitive to the isomer contribution. From the information reported by Pattenden, we find a total cross section of about 34.8 b, which agrees with the value of 35 ± 4 b reported

by Block. However, the values of the capture cross section reported by the two authors exhibit a significant discrepancy. Block deduced a ^{129}I capture cross section of 31 b by assuming a ^{129}I scattering cross section of 4 b, while Pattenden gave a value of 28 ± 2 b, which was deduced from a least-squares fit of the data from 0.01 to 0.7 eV with the equation

$$\sigma_t(E) = \frac{a}{\sqrt{E}} + b, \quad (10)$$

in which a describes the $1/v$ slope of the capture cross section in the thermal energy range and b stands for an energy-independent scattering cross section. A SAMMY calculation with the total cross sections reported by Block and Pattenden, together with our transmission measurement carried out at a 100 Hz repetition rate, gives a capture cross section of about 28.6 b, which is consistent with the result reported by Pattenden. Therefore, there are not many possibilities for improving the trend indicated by these five existing thermal values. In our analysis, we decided to adopt the weighed mean value of 30.0 ± 0.8 b reported in Table III, which is very close to the thermal value reported by Nakamura. With a channel radius $a_c = 6.837$ fm, the posterior negative

TABLE III. ^{129}I thermal capture (σ_γ^{th}) and total (σ_t^{th}) cross sections.

Author	Ref.	Year	σ_t^{th} (barns)
Block	[33]	1960	35 ± 4
Pattenden	[34]	1963	34.8
Author	Ref.	Year	σ_γ^{th} (barns)
Roy	[35]	1958	26.7 ± 2.0
Block	[33]	1960	31.0 ± 4.0
Pattenden	[34]	1963	28.0 ± 2.0
Friedmann	[30]	1983	33.9 ± 1.9
Nakamura	[36]	1996	30.3 ± 1.2
weighed mean value (used in this work)			30.0 ± 0.8

resonances determined with the SAMMY code are

$$\begin{cases} E_-(J^\pi = 4^+) = -21.6 \pm 0.1 \text{ eV}, \\ \Gamma\gamma(J^\pi = 4^+) = 105.9 \pm 3.7 \text{ meV}, \\ \Gamma_n(J^\pi = 4^+) = 64.3 \pm 0.4 \text{ meV}, \end{cases}$$

$$\begin{cases} E_-(J^\pi = 3^+) = -10.7 \pm 0.1 \text{ eV}, \\ \Gamma\gamma(J^\pi = 3^+) = 105.9 \pm 2.4 \text{ meV}, \\ \Gamma_n(J^\pi = 3^+) = 44.7 \pm 0.2 \text{ meV}, \end{cases}$$

and the s -wave effective radius is

$$R'_0 = 5.7 \pm 1.6 \text{ fm}.$$

The R' accuracy cannot be improved because of the low hydrogen, oxygen, and nitrogen mass fraction accuracies. The value of 5.7 fm obtains a good agreement with the experimental total cross sections shown in the lower part of Fig. 2.

C. Internal levels

The resonance parameters were determined with the simultaneous REFIT fitting procedure. The consistency of the results was verified with the SAMMY code. Below 10 keV, we identified 719 resonances for ^{127}I and 399 levels for ^{129}I . This work improves significantly the knowledge of the RRR of the iodine isotopes. The ^{127}I and ^{129}I resonance parameters are given in Tables IV and V up to 1 keV. The complete table of resolved resonance parameters are reported in Ref. [38].

The errors given for the resonance energies take into account the accuracy of the flight path length, the experimental channel widths used to map the entire TOF spectra, the incomplete description of the moderation distance, and the time delay uncertainties. The quoted errors for the radiation widths are only the statistical uncertainties provided by the REFIT code. For the neutron widths, the sources of systematic errors are mainly the sample thickness, the incomplete description of the resolution function, and the time-dependent background. The average systematic error affecting the ^{127}I and ^{129}I neutron width values remains below 3.3% and 3.6%.

This work has confirmed the existence of three small ^{127}I p -wave resonances at 7.5, 10.3, and 13.9 eV. These resonances were previously discovered in the framework of parity violation studies in a compound nucleus [39,40]. The resonance peaks are shown in Fig. 3. The resonance at 7.5 eV is not clearly visible in our spectra. However, a closer inspection of the raw data has indicated the existence of a small structure at the correct neutron energy with an amplitude similar to the ^{127}I resonance peak reported in the literature. Other examples of capture and transmission data are shown in Fig. 4 together with the least-squares adjusted theoretical curves.

D. Spin and parity

For $^{127,129}\text{I}$, the parity of the resonance states cannot be determined from the shape of the resonances. The interference between the potential and the resonant scattering is too small to derive any information. In this work, we have assigned the

TABLE IV. ^{127}I resonance parameters.

E_0 (eV)	J^π	$\Gamma\gamma$ (meV)	$g\Gamma_n$ (meV)
-54.19 ± 0.11	2^+	99.8 ± 1.0	48.462 ± 0.458
-43.31 ± 0.10	3^+	98.3 ± 0.9	65.213 ± 0.583
7.55 ± 0.01	1^-	100.0	0.00012
10.35 ± 0.01	1^-	90.0 ± 5.9	0.003 ± 0.001
13.95 ± 0.01	2^-	99.2 ± 21.2	0.002 ± 0.001
20.38 ± 0.01	2^+	95.7 ± 0.6	0.719 ± 0.024
24.63	1^-	100.0	0.00064
31.21 ± 0.01	3^+	94.7 ± 0.3	9.998 ± 0.290
37.65 ± 0.02	3^+	95.5 ± 0.4	23.250 ± 0.698
39.74 ± 0.02	3^-	96.3 ± 9.6	0.010 ± 0.003
45.31 ± 0.02	2^+	99.8 ± 0.3	9.438 ± 0.302
53.74 ± 0.02	4^-	100.0	0.017 ± 0.001
64.05 ± 0.03	1^-	100.0	0.005 ± 0.001
65.92 ± 0.03	2^+	103.5 ± 10.4	0.911 ± 0.027
78.42 ± 0.04	3^+	102.8 ± 0.5	14.717 ± 0.574
85.76 ± 0.04	3^-	100.0	0.019 ± 0.001
90.40 ± 0.08	3^+	103.8 ± 0.4	10.663 ± 0.373
101.10 ± 0.10	4^-	100.0	0.014 ± 0.001
118.27 ± 0.11	2^-	100.0	0.007 ± 0.001
134.10 ± 0.13	3^-	100.0	0.024 ± 0.002
136.83 ± 0.13	1^-	100.0	0.044 ± 0.002
139.59 ± 0.13	3^+	95.3 ± 0.8	22.819 ± 0.685
145.68 ± 0.14	4^-	100.0	0.036 ± 0.002
153.76 ± 0.14	2^-	100.0	0.101 ± 0.004
159.40 ± 0.15	3^-	100.0	0.007 ± 0.001
167.77 ± 0.16	3^+	100.0	0.585 ± 0.021
168.56 ± 0.16	2^+	105.5 ± 0.5	44.920 ± 1.437
174.09 ± 0.16	2^+	156.9 ± 3.9	1.686 ± 0.059
178.30 ± 0.17	3^+	102.6 ± 4.7	0.450 ± 0.015
195.46 ± 0.18	3^+	102.3 ± 0.5	64.513 ± 1.935
201.10 ± 0.15	4^-	100.0	0.039 ± 0.002
206.34 ± 0.15	2^+	91.4 ± 0.8	19.906 ± 0.916
223.62 ± 0.17	2^-	100.0	0.011 ± 0.001
227.12 ± 0.17	3^-	100.0	0.012 ± 0.001
237.31 ± 0.18	2^+	111.9 ± 1.5	24.419 ± 0.903
244.84 ± 0.18	3^+	124.9 ± 2.4	5.764 ± 0.248
256.68 ± 0.19	4^-	100.0	0.063 ± 0.003
265.23 ± 0.20	3^+	120.4 ± 1.9	20.660 ± 0.930
271.30 ± 0.20	3^+	111.5 ± 3.2	4.252 ± 0.179
274.48 ± 0.20	3^-	100.0	0.023 ± 0.009
282.60 ± 0.21	2^-	100.0	0.011 ± 0.005
292.41 ± 0.22	1^-	100.0	0.143 ± 0.006
299.57 ± 0.22	2^+	111.0 ± 2.2	8.005 ± 0.280
306.44 ± 0.26	4^-	100.0	0.035 ± 0.003
310.85 ± 0.26	2^+	118.6 ± 2.3	10.247 ± 0.400
314.55 ± 0.27	3^-	100.0	0.047 ± 0.004
324.16 ± 0.28	2^+	100.0	0.233 ± 0.010
325.39 ± 0.28	2^+	100.0	0.460 ± 0.017
329.00 ± 0.28	3^+	125.0 ± 7.1	1.673 ± 0.054
346.35 ± 0.29	4^-	100.0	0.122 ± 0.006
351.96 ± 0.30	2^-	100.0	0.093 ± 0.006
353.40 ± 0.30	1^-	100.0	0.094 ± 0.005
362.53 ± 0.31	2^+	143.8 ± 4.7	3.868 ± 0.128
374.74 ± 0.32	2^+	98.9 ± 1.0	67.339 ± 2.020
382.13 ± 0.32	3^-	100.0	0.198 ± 0.011
386.17 ± 0.33	2^+	89.6 ± 0.8	108.425 ± 3.578

TABLE IV. (*Continued.*)

E_0 (eV)	J^π	Γ_γ (meV)	$g\Gamma_n$ (meV)
392.09 ± 0.33	4 ⁻	100.0	0.148 ± 0.012
393.18 ± 0.33	2 ⁻	100.0	0.321 ± 0.016
413.01 ± 0.39	1 ⁻	100.0	0.084 ± 0.009
420.28 ± 0.40	3 ⁺	100.0	13.976 ± 0.629
421.85 ± 0.40	3 ⁻	100.0	0.186 ± 0.016
426.93 ± 0.40	2 ⁺	99.4 ± 0.7	60.547 ± 1.816
431.40 ± 0.41	4 ⁻	100.0	0.148 ± 0.010
434.95 ± 0.41	3 ⁺	100.9 ± 2.0	27.234 ± 1.334
440.06 ± 0.41	2 ⁻	100.0	0.187 ± 0.010
448.27 ± 0.42	2 ⁺	117.9 ± 1.5	26.581 ± 1.143
454.78 ± 0.43	3 ⁺	100.0	0.677 ± 0.023
458.30 ± 0.43	1 ⁻	100.0	0.104 ± 0.017
468.42 ± 0.44	3 ⁻	100.0	0.128 ± 0.013
475.81 ± 0.45	2 ⁺	107.5 ± 5.5	5.350 ± 0.203
480.09 ± 0.45	2 ⁺	115.1 ± 4.4	8.176 ± 0.270
499.39 ± 0.47	2 ⁺	128.6 ± 2.4	23.244 ± 0.790
515.35 ± 0.53	2 ⁺	121.1 ± 3.3	23.131 ± 0.810
518.16 ± 0.53	3 ⁺	110.5 ± 4.0	19.628 ± 0.746
533.34 ± 0.55	3 ⁺	100.6 ± 1.4	59.322 ± 2.136
545.97 ± 0.56	4 ⁻	100.0	0.128 ± 0.013
550.50 ± 0.57	2 ⁺	100.0	0.632 ± 0.023
563.07 ± 0.58	3 ⁻	100.0	0.478 ± 0.028
565.92 ± 0.58	3 ⁺	99.2 ± 1.8	87.437 ± 2.711
569.14 ± 0.59	2 ⁺	94.7 ± 6.0	10.626 ± 0.383
578.71 ± 0.60	2 ⁻	100.0	0.321 ± 0.016
584.28 ± 0.60	2 ⁺	100.0	2.012 ± 0.066
588.72 ± 0.61	4 ⁻	100.0	0.233 ± 0.012
596.58 ± 0.61	1 ⁻	100.0	0.128 ± 0.013
619.22 ± 0.69	3 ⁺	95.5 ± 2.1	36.707 ± 1.321
624.30 ± 0.69	3 ⁻	100.0	0.707 ± 0.028
632.55 ± 0.70	3 ⁺	97.3 ± 3.4	21.401 ± 0.792
635.75 ± 0.71	4 ⁻	100.0	0.386 ± 0.024
643.63 ± 0.71	2 ⁻	100.0	0.514 ± 0.115
644.73 ± 0.72	2 ⁺	84.9 ± 11.6	5.534 ± 0.216
646.99 ± 0.72	1 ⁻	100.0	0.150 ± 0.016
658.85 ± 0.73	3 ⁺	126.0 ± 9.4	3.971 ± 0.131
662.36 ± 0.74	3 ⁻	100.0	0.405 ± 0.019
669.30 ± 0.74	2 ⁺	98.6 ± 2.3	30.011 ± 1.110
690.11 ± 0.77	3 ⁺	100.0	0.892 ± 0.033
702.09 ± 0.84	3 ⁺	101.3 ± 2.0	64.046 ± 2.049
708.41 ± 0.84	2 ⁺	87.2 ± 5.1	104.954 ± 8.501
708.71 ± 0.84	3 ⁺	98.5 ± 4.2	123.342 ± 7.401
714.03 ± 0.85	4 ⁻	100.0	0.145 ± 0.034
726.75 ± 0.86	2 ⁻	100.0	0.358 ± 0.024
730.92 ± 0.87	2 ⁺	97.4 ± 1.9	61.130 ± 2.017
734.47 ± 0.87	3 ⁻	100.0	0.482 ± 0.027
744.49 ± 0.89	3 ⁺	97.7 ± 1.5	109.544 ± 3.505
757.92 ± 0.90	4 ⁻	100.0	0.690 ± 0.034
762.49 ± 0.91	2 ⁺	99.0 ± 1.6	111.759 ± 3.688
767.08 ± 0.91	1 ⁻	100.0	0.379 ± 0.026
772.14 ± 0.92	2 ⁻	100.0	0.082 ± 0.015
777.30 ± 0.92	3 ⁻	100.0	0.168 ± 0.021
779.76 ± 0.93	3 ⁺	100.0	4.199 ± 0.147
790.64 ± 0.94	3 ⁺	106.8 ± 6.5	10.925 ± 0.371
796.74 ± 0.95	4 ⁻	100.0	0.075 ± 0.008
805.45 ± 0.43	1 ⁻	100.0	0.420 ± 0.021

TABLE IV. (*Continued.*)

E_0 (eV)	J^π	Γ_γ (meV)	$g\Gamma_n$ (meV)
813.40 ± 0.44	2 ⁺	103.1 ± 2.3	38.870 ± 1.360
818.13 ± 0.44	2 ⁻	100.0	0.255 ± 0.018
828.16 ± 0.45	3 ⁺	136.1 ± 6.4	6.504 ± 0.247
834.06 ± 0.45	3 ⁺	92.7 ± 1.7	88.428 ± 2.918
840.01 ± 0.45	4 ⁻	100.0	0.395 ± 0.026
862.47 ± 0.47	3 ⁺	124.7 ± 11.8	6.737 ± 0.236
867.44 ± 0.47	3 ⁻	100.0	0.665 ± 0.029
890.56 ± 0.48	2 ⁺	112.5 ± 7.1	10.651 ± 0.341
898.05 ± 0.48	4 ⁻	100.0	0.176 ± 0.025
901.69 ± 0.50	2 ⁺	131.5 ± 8.9	11.230 ± 0.371
915.18 ± 0.50	3 ⁺	101.8 ± 7.9	13.002 ± 0.416
918.21 ± 0.51	3 ⁻	100.0	0.517 ± 0.037
920.02 ± 0.51	2 ⁻	100.0	0.310 ± 0.033
925.27 ± 0.51	1 ⁻	100.0	0.454 ± 0.027
927.99 ± 0.51	4 ⁻	100.0	0.951 ± 0.041
943.26 ± 0.52	3 ⁺	161.2 ± 5.5	29.597 ± 0.977
955.23 ± 0.53	3 ⁺	96.6 ± 2.2	79.095 ± 2.610
961.30 ± 0.53	3 ⁺	101.7 ± 9.1	12.191 ± 0.402
966.48 ± 0.53	4 ⁻	100.0	0.725 ± 0.037
969.68 ± 0.53	3 ⁻	100.0	0.140 ± 0.026
972.14 ± 0.53	2 ⁻	100.0	0.497 ± 0.031
987.44 ± 0.54	1 ⁻	100.0	0.972 ± 0.039
1003.80 ± 0.56	4 ⁻	100.0	0.967 ± 0.083

parity of the resonances with a statistical test implemented in the ESTIMA code [41]. The approach couples the statistical spin assignment derived from the work of Bollinger and Thomas [42] and the properties of the Porter-Thomas reduced neutron width distribution [11]. The adequate distribution for the reduced neutron width Γ_n^l is a χ^2 function with one degree of freedom:

$$P(x) dx = \frac{e^{-\frac{x}{2}}}{\sqrt{2\pi x}}. \quad (11)$$

For s -wave levels ($l = 0$), the dimensionless variable x is expressed as

$$x = \frac{g_J \Gamma_n^0}{\langle g_J \Gamma_n^0 \rangle}, \quad \text{with } \Gamma_n^0 = \Gamma_n \sqrt{\frac{1 \text{ eV}}{E}}, \quad (12)$$

$\langle g_J \Gamma_n^0 \rangle$ is the average s -wave reduced neutron width, and Γ_n stands for the neutron width. The statistical spin factor g_J gives the probability of getting the allowed total angular momentum J from the intrinsic spins of the target nucleus I and of the incident particle i , that is,

$$g_J = \frac{2J + 1}{(2i + 1)(2I + 1)}. \quad (13)$$

The ESTIMA method allows us to distinguish resonances with $l = 0$ and $l = 1$, according to their neutron width values. The probability $P(l = 1 | g_J \Gamma_n)$ that a resonance is a p -wave given its $g_J \Gamma_n$ can be expressed in terms of conditional probabilities. A detailed description of the formalism based on the Bayes theorem and applied to neutron resonance spectroscopy can be found elsewhere [5,43]. In ESTIMA, this

TABLE V. ^{129}I resonance parameters.

E_0 (eV)	J^π	Γ_γ (meV)	$g\Gamma_n$ (meV)
-21.60 ± 0.10	4^+	105.9 ± 3.7	36.169 ± 0.225
-10.70 ± 0.10	3^+	105.9 ± 2.4	19.556 ± 0.087
41.37 ± 0.02	4^+	94.9 ± 6.6	0.069 ± 0.003
72.13 ± 0.03	3^+	90.8 ± 0.6	7.324 ± 0.249
76.15 ± 0.03	4^+	106.0	0.058 ± 0.003
96.36 ± 0.09	4^+	104.9 ± 2.9	0.756 ± 0.026
115.19 ± 0.11	2^-	106.0	0.028 ± 0.002
128.32 ± 0.12	3^+	97.9 ± 1.3	3.832 ± 0.130
140.63 ± 0.13	3^-	106.0	0.055 ± 0.029
146.40 ± 0.14	3^+	108.5 ± 0.9	23.109 ± 0.786
152.57 ± 0.14	3^+	105.4 ± 0.8	12.123 ± 0.424
164.96 ± 0.16	4^-	106.0	0.049 ± 0.004
198.75 ± 0.19	4^+	140.0 ± 4.3	2.037 ± 0.073
202.67 ± 0.15	3^-	106.0	0.026 ± 0.004
259.16 ± 0.19	4^+	106.0	0.884 ± 0.032
265.38 ± 0.20	3^-	106.0	0.234 ± 0.032
284.17 ± 0.21	3^+	107.4 ± 2.4	7.389 ± 0.251
290.65 ± 0.22	3^+	109.8 ± 2.2	8.951 ± 0.304
295.60 ± 0.22	3^+	106.0	1.568 ± 0.055
314.05 ± 0.27	4^-	106.0	0.205 ± 0.020
315.97 ± 0.27	3^-	106.0	0.266 ± 0.020
348.88 ± 0.30	2^-	106.0	0.142 ± 0.011
353.85 ± 0.30	4^+	106.0	0.547 ± 0.051
356.23 ± 0.30	3^+	106.0	0.824 ± 0.037
360.70 ± 0.31	4^-	106.0	0.153 ± 0.024
364.89 ± 0.31	4^+	106.0	1.649 ± 0.221
410.04 ± 0.39	3^+	114.4 ± 1.4	33.565 ± 1.141
423.23 ± 0.40	3^+	123.6 ± 1.2	57.925 ± 1.969
454.28 ± 0.43	3^+	109.6 ± 1.5	28.232 ± 0.960
469.24 ± 0.44	3^+	107.4 ± 1.1	67.331 ± 2.289
489.31 ± 0.46	3^+	127.0 ± 1.8	32.528 ± 1.106
492.73 ± 0.46	3^-	106.0	0.383 ± 0.027
511.64 ± 0.53	3^-	106.0	0.249 ± 0.026
524.45 ± 0.54	2^-	106.0	0.399 ± 0.144
547.98 ± 0.56	3^+	101.1 ± 9.1	31.706 ± 1.078
554.71 ± 0.57	3^+	106.0	0.830 ± 0.091
562.09 ± 0.58	3^-	106.0	0.158 ± 0.027
576.79 ± 0.59	4^-	106.0	0.279 ± 0.045
578.53 ± 0.60	3^-	106.0	0.384 ± 0.036
595.58 ± 0.61	4^+	106.0	6.249 ± 0.219
654.54 ± 0.73	4^+	106.0	1.977 ± 0.087
689.63 ± 0.77	4^-	106.0	0.557 ± 0.056
693.26 ± 0.77	4^+	110.2 ± 1.2	111.600 ± 3.794
719.66 ± 0.86	4^+	106.0	21.673 ± 0.759
725.35 ± 0.86	3^-	106.0	0.220 ± 0.028
730.17 ± 0.87	2^-	106.0	0.175 ± 0.068
761.56 ± 0.91	4^+	106.0	5.560 ± 0.211
797.09 ± 0.95	3^+	104.1 ± 1.2	90.256 ± 3.069
803.65 ± 0.43	3^+	122.6 ± 2.1	55.737 ± 1.895
842.43 ± 0.45	3^-	106.0	0.322 ± 0.032
845.69 ± 0.46	3^-	106.0	0.146 ± 0.029
855.25 ± 0.46	3^+	106.3 ± 1.7	58.319 ± 1.983
866.93 ± 0.47	4^-	106.0	0.566 ± 0.057
879.28 ± 0.47	2^-	106.0	0.482 ± 0.036
888.46 ± 0.48	3^+	106.0	6.055 ± 0.224
897.42 ± 0.48	3^-	106.0	0.178 ± 0.029

TABLE V. (Continued.)

E_0 (eV)	J^π	Γ_γ (meV)	$g\Gamma_n$ (meV)
915.31 ± 0.50	3^+	96.7 ± 1.3	116.550 ± 3.963
926.06 ± 0.51	3^+	106.0	3.658 ± 0.172
969.36 ± 0.53	4^-	106.0	0.789 ± 0.060
991.31 ± 0.55	3^-	106.0	0.542 ± 0.052
1002.75 ± 0.56	3^+	132.9 ± 1.6	169.619 ± 5.767

statistical test is used in association with a method based on the truncated Porter-Thomas distribution. The method gives the number of s -wave resonances $N(x_0)$ having an x value larger than a threshold x_0 . $N(x_0)$ is obtained by integrating Eq. (11) as

$$N(x_0) = N \int_{x_0}^{\infty} P(x) dx = N \left(1 - \operatorname{erf} \sqrt{\frac{x_0}{2}} \right), \quad (14)$$

in which N stands for the number of s -wave resonances. In practice, resonances characterized by a small reduced neutron width and a high $P(l=1|g_J\Gamma_n)$ value, which deviate significantly from the theoretical curve [Eq. (14)], are assumed to be p -wave resonances. By iterating the code, we are able to suggest a “confident” sample of s -wave resonances. The results are presented in Fig. 5 in terms of $g_J\Gamma_n/\sqrt{E}$ values.

Similarly, the experimental assessment of the total angular momentum of the $^{127,129}\text{I}$ resonances was not possible. The quantity extracted from our data is $g_J\Gamma_n$, instead of Γ_n . Therefore, we used the nuclear data processing system CALENDF [44] to perform a statistical assignment of the J values for $l=0$ and $l=1$. The suggestion proposed by the code is based on the Gilbert and Cameron level density formula (see Appendix) in association with the Wigner level spacing distribution [10].

E. Iodine 127

The ^{127}I resonance parameters available in the neutron databases are mainly taken from three earlier TOF measurements. In 1965, the total cross section was investigated by Garg *et al.* (up to 500 keV) at a 200 m flight path of the Columbia University synchro-cyclotron, using three transmission samples of solid elemental iodine (9.3×10^{-2} , 2.0×10^{-2} , and 3.5×10^{-3} at/b) [46]. Some ten years later, in 1976, a series of capture, self-indication, and transmission measurements were carried out at a 60 m flight path of the GELINA facility by Rohr *et al.*, using three PbI_2 samples (1.236×10^{-2} , 2.485×10^{-3} , and 7.438×10^{-3} at/b), within the 20 eV to 5.0 keV energy range [47]. Finally, in 1983, Macklin determined the capture cross section at the ORELA facility from 2.5 to 500 keV, using a PbI_2 sample having dimensions of $20 \times 52 \times 1.6$ mm and weighing 11.91 g [1].

We have compared our ^{127}I results with the reduced neutron widths ($g_J\Gamma_n^0$), with the $g_J\Gamma_n$ values, and with the capture areas [$A_\gamma = g_J\Gamma_n\Gamma_\gamma/(\Gamma_n + \Gamma_\gamma)$] reported, respectively, by Garg *et al.*, Rohr *et al.*, and Macklin. The ratios of these quantities as a function of the neutron energy are shown, respectively, in Figs. 6, 7, and 8. The results given by Garg *et al.* are affected

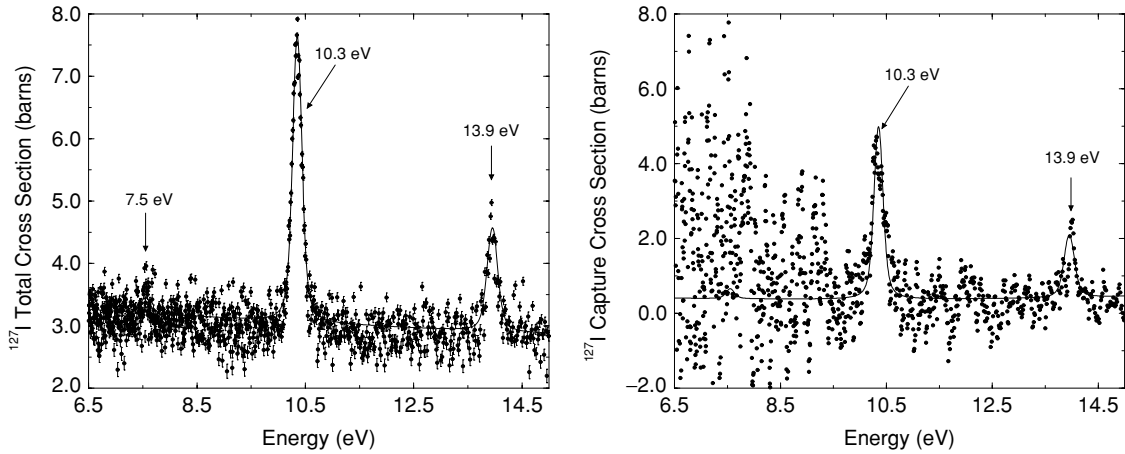


FIG. 3. Low neutron energy range of the ^{127}I total and capture cross sections measured in this work. Three small p -wave resonances at 7.5, 10.3, and 13.9 eV were previously reported in Refs. [38,39]. For the capture measurement, the cutoff energy of the thick boron antioverlap filter was close to 9.5 eV. Below this lower energy limit, the noisy values have to be disregarded.

by a systematic error of about 13%, possibly due to the use of unstable elemental iodine samples. The distribution obtained with the results from Macklin is centered around 1.07 and has a large standard deviation of 0.23. The largest part of this bias can be explained by the thickness and normalization uncertainties. Indeed, an overall accuracy better than 5% cannot be achieved from the analysis of a single capture measurement performed with a very thin sample in powder form. The best agreement is obtained with the results obtained more than 20 years ago at

the IRMM. Below 1 keV, the discrepancy between the $g_J\Gamma_n$ values reported by Rohr *et al.* and determined in this work averages about 2%.

F. Iodine 129

Very little experimental work is available on neutron cross sections of ^{129}I . The first five s -wave resonances were reported in 1963 by Pattenden [34]. The Γ_n values were derived from

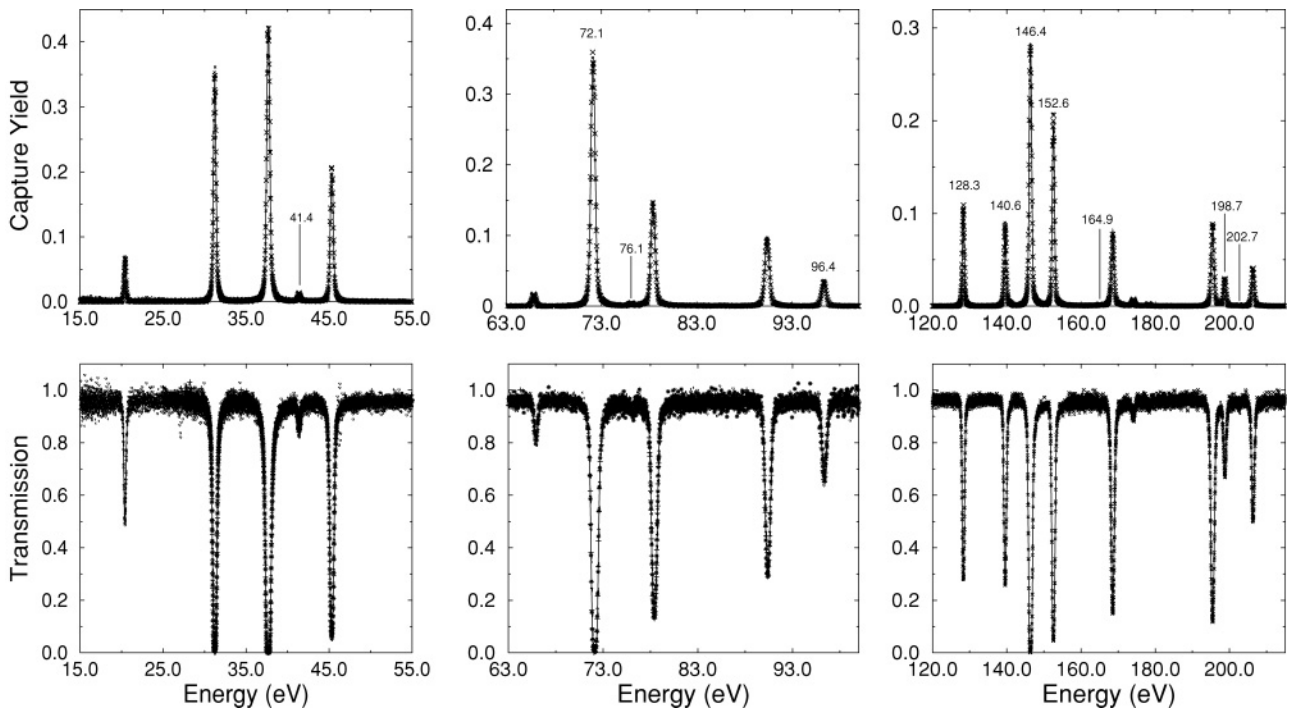


FIG. 4. Examples of $^{127,129}\text{I}$ resonance peaks observed below 200 eV. Transmission data were obtained with the thick $\text{Pb}^{127,129}\text{I}_2$ sample [$n(^{129}\text{I}) = 1.465 \times 10^{-3}$ at/b]. Capture yield was measured with the thin $\text{Pb}^{127,129}\text{I}_2$ sample [$n(^{129}\text{I}) = 1.564 \times 10^{-4}$ at/b]. Solid line is the least-squares adjusted theoretical curve calculated with the REFIT code. Energies of the ^{129}I resonances are indicated on the figures. Other resonances are those of the ^{127}I isotope.

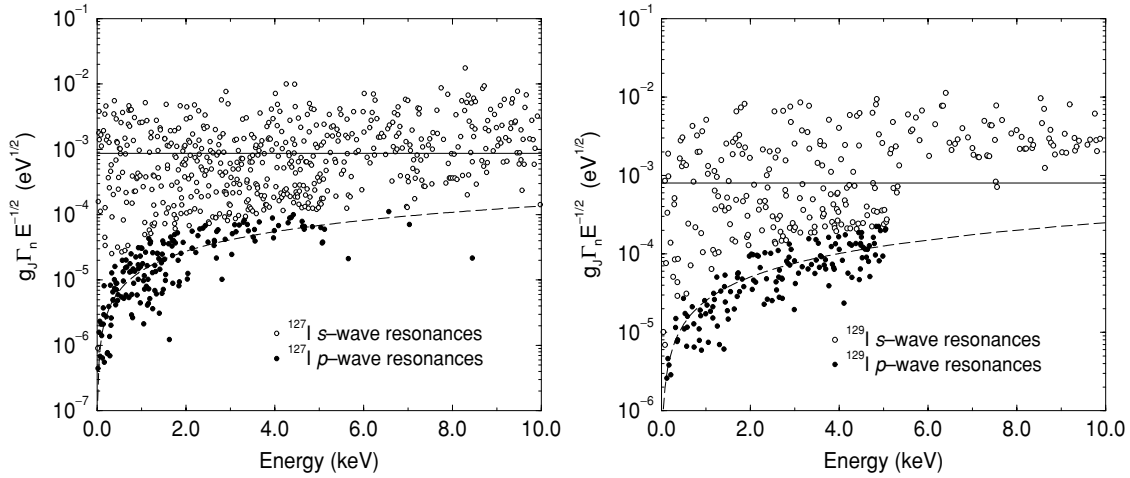


FIG. 5. $^{127,129}\text{I}$ neutron widths in terms of $g\Gamma_n/\sqrt{E}$ as a function of the resonance energies. The results are divided into s - and p -wave resonances as suggested by the ESTIMA code [41]. Solid and dashed lines, respectively, represent the average values.

transmission measurements carried out at the ORNL chopper assuming a mean radiation width of 100 meV. This value is in excellent agreement with the mean radiation width of 106 meV obtained in this work.

Some 20 years later, neutron capture by ^{129}I was reported by Macklin [1]. The capture measurements were carried out at the ORELA up to 500 keV with a PbI_2 sample having dimensions of $26 \times 52 \times 2$ mm and weighing 18.76 g. The ^{129}I content (1.3×10^{-3} at/b) was determined by comparison of the sample radioactivity with an Amersham standard. The thickness accuracy reported by Macklin is about 3%.

In Fig. 9, we compare the ^{129}I capture areas [$A_\gamma = g_J\Gamma_n\Gamma_\gamma/(\Gamma_n + \Gamma_\gamma)$] reported by Macklin with the present results. The mean discrepancy between the two data sets is about 3.6%. However, for the first broad s -wave resonance at 72.1 keV, the discrepancy reaches 10%. The largest part of this discrepancy probably comes from the data processing and the resonance peak parametrization. Macklin fitted the neutron capture peaks of ^{129}I with single-level Breit-Wigner parameters, assuming throughout an average s -wave spin

factor $g_J = 0.5$. Moreover, above 2 keV, the capture areas were analyzed using sample data from which the ^{127}I contribution had been subtracted. Final results from this approach are often questionable because of resonance overlaps, the effect of the resolution function, and the use of prior multiple scattering corrections. The SAMMY and REFIT codes include these experimental corrections in the fitting procedure. The present set of ^{129}I resonance parameters is then the first to be extracted over a wide energy range with modern resonance shape analysis techniques.

V. THE UNRESOLVED RESONANCE RANGE

A. Prior s -wave average parameters

Reliable prior information on the average parameters can be obtained from the statistical analysis of the resolved resonance parameters. The prior s -wave parameters of interest for this work are the mean radiation width $\langle\Gamma_\gamma\rangle$, the mean level

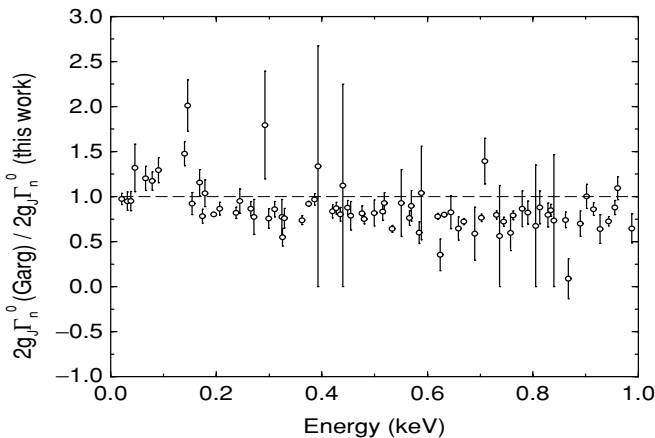


FIG. 6. Comparison between the ^{127}I reduced neutron widths from Garg *et al.* [46] and our results.

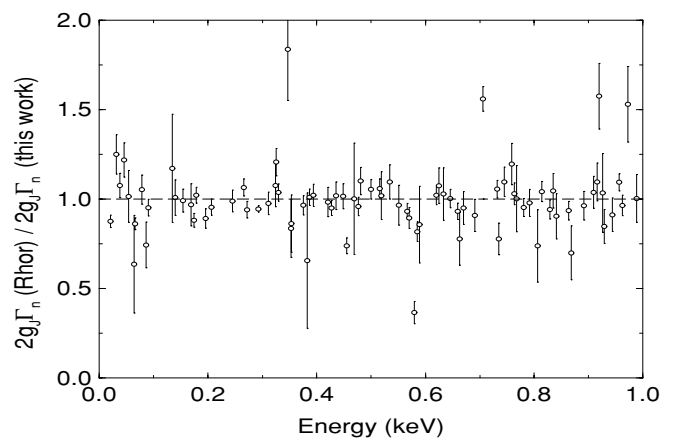


FIG. 7. Comparison between the ^{127}I neutron widths from Rohr *et al.* [47] and our results.

TABLE VI. ^{127}I and ^{129}I average parameters deduced from statistical analysis of individual resonance parameters. Fermion gas level density parameter a was deduced from the D_0 value, and the p -wave mean level spacing D_1 was calculated with the Gilbert and Cameron level density formula [45].

Average resonance parameters		Iodine 127	Iodine 129
s -wave neutron strength function	$10^4 S_0$	0.72 ± 0.06	0.54 ± 0.07
s -wave distant level parameter	R_0^∞	0.19 ± 0.01	$\simeq 0.16$
Average radiation width (meV)	$\langle \Gamma \gamma_0 \rangle$	100.0 ± 22.6	106.0 ± 15.2
s -wave mean level spacing (eV)	D_0	12.5 ± 0.3	27.3 ± 0.9
p -wave mean level spacing (eV)	D_1	6.5 ± 0.1	14.1 ± 0.5
Level density parameter (MeV^{-1})	a	17.42 ± 0.04	16.56 ± 0.06

spacing D_0 , the strength function S_0 , and the distant level parameter R_0^∞ . Our results are reported in Table VI.

In practice, $\langle \Gamma \gamma_0 \rangle$ and R_0^∞ are deduced from the results of the resonance shape analysis. The mean radiation width is defined as the weighted average value of the individual radiation widths and R_0^∞ is defined as a function of the potential scattering length R'_0 and of the channel radius a_c [48]:

$$R_0^\infty = 1 - \frac{R'_0}{a_c}. \quad (15)$$

The prior s -wave mean level spacing D_0 is deduced from the number of levels N [Eq. (14)] determined in a given interval ΔE by accounting for missing weak levels:

$$D_0 = \frac{\Delta E}{N}. \quad (16)$$

The mean level spacings for higher order partial waves ($l = 1, 2, \dots$) are calculated with the Gilbert and Cameron level density formula [45], for which the fermion gas level

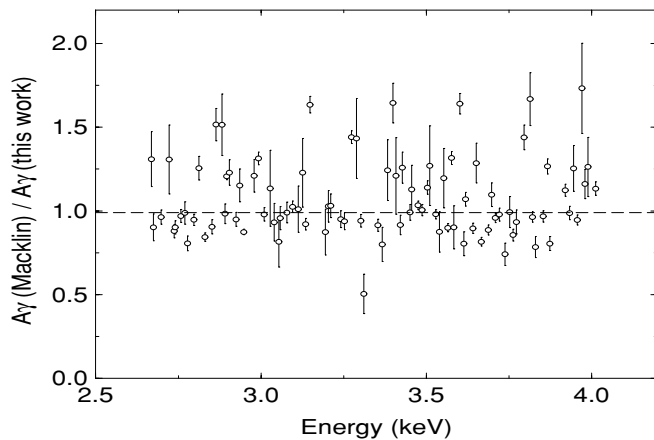


FIG. 8. Comparison between the ^{127}I capture areas from Macklin [1] and our results.

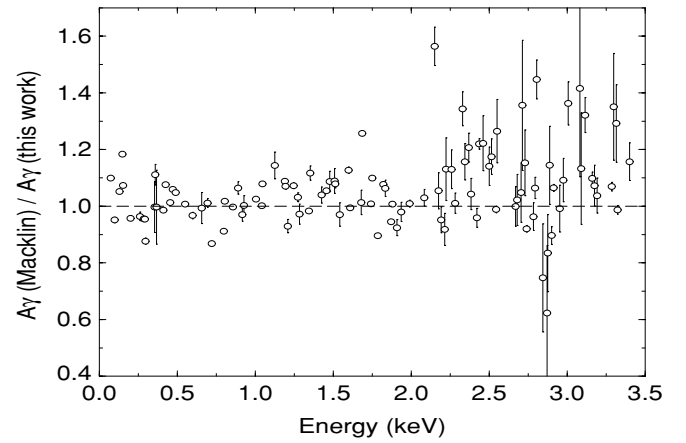


FIG. 9. Comparison between the ^{129}I capture areas given by Macklin [1] and the present values.

density parameter a plays a crucial role. The formula used in this work is given in the Appendix.

The neutron strength function S_0 is closely related to the transmission coefficients $T_{l=0}$ obtained with optical model calculations. For the s -wave channel, S_0 can be expressed as

$$S_0 \simeq \frac{T_{l=0}}{2\pi\sqrt{E}}. \quad (17)$$

Alternatively, S_0 is defined as the ratio of the average s -wave reduced neutron width [Eq. (12)] to the s -wave mean level spacing [Eq. (16)]:

$$S_0 = \frac{\langle g_J \Gamma_n^0 \rangle}{D_0}. \quad (18)$$

Careful determination of prior ^{129}I average parameters has never been performed. In the main neutron databases, ^{129}I resonances are assumed to be s waves with spin and parity 3^+ and 4^+ . Parameters of the resonances were produced with the capture area values reported by Macklin [1]. Therefore, earlier statistical calculations were mostly based on nuclear systematics.

The mean radiation widths reported in Table VI are the weighted average values of the $\Gamma\gamma$ determined from simultaneous analysis of the transmission and capture data. We have extracted the ^{127}I and ^{129}I radiation widths for, respectively, 155 and 55 resonances. The quoted uncertainties are the standard deviations of the distributions of the fitted values. The R_0^∞ values were deduced from the effective potential scattering lengths R'_0 given in Sec. IV B. D_0 and S_0 were determined by accounting for the missing weak levels with the ESTIMA method [Eq. (14)].

Histograms of the distributions of the dimensionless variable $g_J \Gamma_n^0 / \langle g_J \Gamma_n^0 \rangle$ and of the next-neighbor spacing for the ^{127}I and ^{129}I s -wave resonances are shown in Fig. 10. The distribution are compared with the theoretical curves calculated with the s -wave strength functions and mean level spacings reported in Table VI. The reduced neutron width distributions are in satisfactory agreement with the theoretical curve hypothesized by Porter and Thomas [Eq. (11)]. The comparison between the level spacing distributions and the Wigner law for a two-spin sequence shows that the agreement

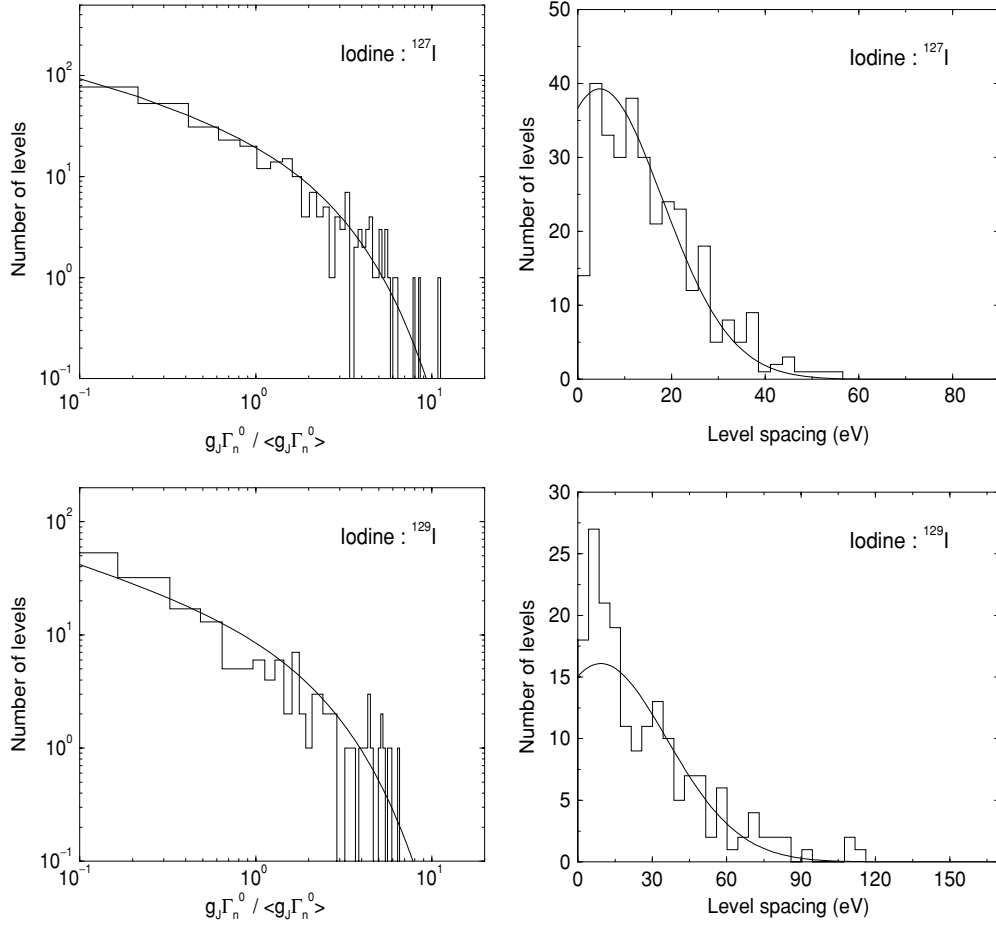


FIG. 10. Comparison between the experimental (histogram) and calculated (smooth curve) reduced neutron width and next-neighbor level spacing distributions. Histograms account for the s -wave resonances up to 5 keV, regardless of the total angular momentum. Smooth curve values were calculated with the parameters reported in Table VI.

for high spacings is much better than that for spacing values lower than D_0 . For low spacing values, the histograms are altered by missing weak levels and “contamination” of higher order partial waves. The latter contribution depends on the criteria chosen to distinguish the s - and p -wave levels. As mentioned in Ref. [5], the condition $P(l = 0 | g_J \Gamma_n) = P(l = 1 | g_J \Gamma_n)$ corresponds to a diffuse region that influences the parity assignment and the level density.

B. Hauser-Feshbach analysis

The interpretation of the URR in terms of level-statistical parameters (strength function S_l , mean level spacing D_l , mean radiation width $\langle \Gamma \gamma_l \rangle$, and distant level parameter R_l^∞) was performed with the FITACS option of the SAMMY code [14,49]. In this code, the modeling of the average partial cross sections is based on the Hauser-Feshbach formula with width fluctuations. The energy dependence of the average radiation width is calculated via a giant dipole resonance (GDR) representation in the form of a classical Lorentz line. The mean level spacings are calculated with the Gilbert and Cameron level density formula given in the Appendix.

The modeling of the average total cross section depends on the resonance-average collision function, which describes the nuclear interaction for a given ingoing ($c = \{l, s, J\}$) and outgoing ($c' = \{l', s', J'\}$) wave function. Its coefficients $\overline{S}_{cc'}$ are closely related to the S -matrix elements used in optical model calculations. The average total cross section for a given angular momentum, parity, and incident channel c is a linear function of \overline{S}_{cc} , that is,

$$\overline{\sigma}_c(E) = 2\pi\lambda^2 g_J [1 - \mathcal{R}e \overline{S}_{cc}(E)], \quad (19)$$

with

$$\overline{S}_{cc}(E) = \exp(-2i\varphi_c) \left[\frac{1 + iP_c(E)[R_c^\infty + i\pi s_c(E)]}{1 - iP_c(E)[R_c^\infty + i\pi s_c(E)]} \right], \quad (20)$$

where φ_c stands for the phase shift of hard-sphere scattering, P_c is the penetration factor, R_c^∞ is the distant level parameter (related to the effective radius R'_c), and s_c is the so-called pole strength function, which may be expressed in terms of strength function S_c as

$$s_c(E) = \frac{S_c \sqrt{E}}{2k a_c}. \quad (21)$$

For modeling the average partial cross sections, the formalism used in this work is based on an elaborate form of the Hauser-Feshbach formula proposed by Moldauer [50,51]. The partial cross section in terms of transmission coefficients T_c is given by

$$\begin{aligned} \overline{\sigma_{cc'}}(E) = & \sigma_p \delta_{cc'} + \pi \bar{\lambda}^2 g_J \frac{T_c(E) T_{c'}(E)}{\sum_c T_c(E)} \times \left(1 + \frac{2}{\bar{\nu}_c} \delta_{cc'} \right) \\ & \times \int_0^\infty \prod_{c''} \left(1 + \frac{2T_{c''}(E)}{\bar{\nu}_{c''} \sum_c T_c(E)} x \right)^{-\delta_{cc''} - \delta_{c''c'} - \bar{\nu}_{c''}/2} dx. \end{aligned} \quad (22)$$

The first term of this equation accounts for the potential scattering cross section σ_p . The second term represents the pure Hauser-Feshbach formula. The other terms are correction factors. The $\bar{\nu}_c$ parameter stands for the effective degree of freedom for the generalized Porter-Thomas distribution of the partial widths. According to the Moldauer prescription, based on Monte Carlo simulations, $\bar{\nu}_c$ has to be taken as [51]

$$\bar{\nu}_c = [1.78 + (T_c^{1.218} - 0.78)e^{-0.228 \sum_c T_c}] \nu_c. \quad (23)$$

For the neutron channel, the degree of freedom ν_c is equal to unity. In the case of photon channels, owing to the usually large number of allowed radiative transitions, ν_c tends toward infinity.

In the pure Hauser-Feshbach formula [52], the resonant structures are described in a single-level Breit-Wigner approximation, under the restriction that all partial widths are smaller than the level spacing (isolated resonance), and assuming no correlation between the partial widths of different channels. The generalization of the formalism for significant level overlap involves two extra factors. In Eq. (22), the first pair of parentheses accounts for the channel-channel correlations, namely, “elastic enhancement” [53]. This correction is of particular importance for the evaluation of elastic cross sections ($c = c'$). Its value is expected to be limited to a factor of 2 to 3. Its importance becomes negligible for nonelastic cross sections when there is a large number of open channels. The second correction factor in Eq. (22) is the integrand known as the Dresner factor. It is a width fluctuation correction that accounts for the multilevel interferences.

C. Averaged ^{127}I and ^{129}I cross sections

Hauser-Feshbach analysis has been performed from 3.5 keV to 1 MeV for ^{127}I and from 3.5 to 100 keV for ^{129}I . The energetically allowed reactions are radiative capture, elastic scattering, and inelastic scattering.

Our FITACS results are presented in Fig. 11 together with our data averaged over a broad energy mesh. The theoretical curves have been obtained with a simultaneous FITACS fit performed over three transmission and two capture data sets. Owing to the resonances of the natural lead (and of the sulfur filter which was kept permanently in the neutron beam), averaged pointwise capture data in the vicinity of 35 keV were left out of our analysis. The arrows indicate the Wigner cusp that corresponds to the increasing competition of the inelastic scattering above 57.6 keV (^{127}I) and 27.8 keV (^{129}I).

TABLE VII. ^{127}I and ^{129}I average resonance parameters determined in the URR with the FITACS option of the SAMMY code. $S_{l=0,1}$ stands for the neutron strength function, $R_{l=0,1}^\infty$ is the so-called distant level parameter, and $\langle \Gamma \gamma_{l=0,1} \rangle$ represents the mean radiation width. Quoted uncertainties are the statistical errors given by SAMMY.

Parameters	Iodine 127	Iodine 129
<i>s</i> -wave		
$10^4 S_0$	0.78 ± 0.01	0.58 ± 0.01
R_0^∞	0.19 ± 0.01	0.17 ± 0.01
$\langle \Gamma \gamma_0 \rangle$ (meV)	112.4 ± 0.1	108.3 ± 0.9
<i>p</i> -wave		
$10^4 S_1$	1.53 ± 0.01	1.41 ± 0.13
R_1^∞	-0.13 ± 0.01	-0.11 ± 0.01
$\langle \Gamma \gamma_1 \rangle$ (meV)	103.2 ± 0.1	114.2 ± 1.4

For ^{127}I , experimental total cross sections covering the 4–25 keV energy range have never been reported in the literature. ^{127}I average resonance parameters recommended in the neutron databases were often deduced from partial cross sections or adjusted to smoothly join the RRR and the experimental data above 100 keV. Similarly, before the present work, experimental data were not available for the ^{129}I total cross section above the resonance region. Previous ^{129}I strength functions were obtained with optical model calculations by assuming the magnitudes of the ^{127}I and ^{129}I total cross sections to be comparable. This work is then the first to cover a wide energy range from subthermal to high energy ranges.

The *s*- and *p*-wave Hauser-Feshbach parameters, adjusted on the present data, are listed in Table VII. A closer inspection of the *s*-wave parameters shows that the neutron strength function S_0 and the distant level parameter R_0^∞ determined in the URR are in good agreement with those obtained in the RRR (Table VI). The discrepancies between the ^{127}I and ^{129}I *s*-wave strength functions are, respectively, 8.2% and 7.4%. This result ensures a satisfactory consistency between the Reich-Moore and Hauser-Feshbach models.

For the *s*-wave mean radiation widths, we obtained an excellent agreement between the ^{129}I results determined in the resolved and unresolved resonance ranges. The discrepancy is lower than 2.5%. For ^{127}I , the *s*-wave average radiation width is 12.4 meV higher than the value obtained in the RRR (Table VI). Although this result remains consistent with the standard deviation (=22.6 meV) of the distribution of the $\Gamma \gamma$ values, it shows how difficult the reliable discrimination of *l*-dependent statistical parameters is.

Table VIII presents the ^{127}I and ^{129}I average capture cross sections calculated with the nuclear data processing system NJOY at 293.6 K. For practical purposes, we have chosen to present the results in a broad energy group structure. The quoted uncertainties account for the accuracy of the sample composition, background, and normalization. The final systematic errors on the ^{127}I and ^{129}I average capture cross sections are, respectively, close to 3.7% and 5.0%. For comparison, the systematic uncertainty which affects the accuracy of the ^{127}I total cross section is lower than 4.2%. In

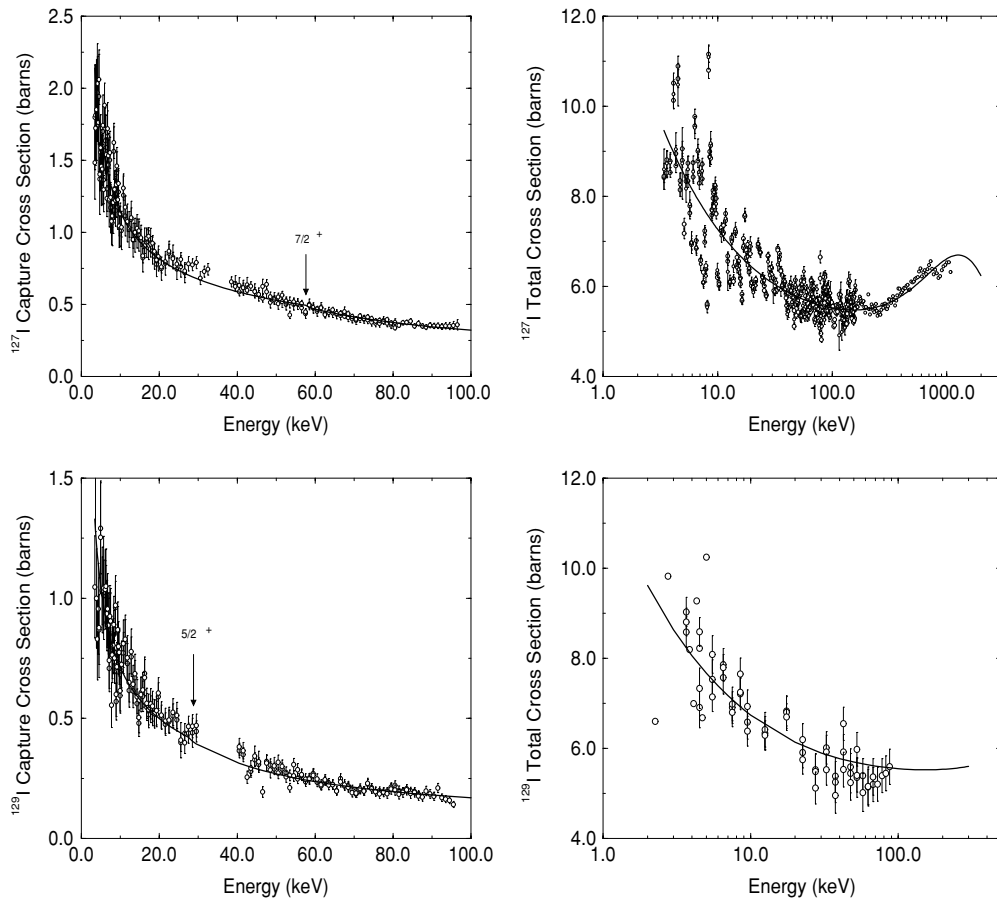


FIG. 11. Experimental ^{127}I and ^{129}I capture and total cross sections in the unresolved resonance range. Solid lines stand for the least-squares adjusted theoretical curves calculated with the FITACS option of the SAMMY code [14]. Arrows indicate the inelastic thresholds.

contrast, the error on the ^{129}I total cross section ranges from 10% to 20%. A better accuracy cannot be achieved without an improved knowledge of the complex sample composition.

D. Statistical model parameters

In this section, special care is given to the trend of the model parameters with respect to the mass number of the compound nucleus. The parameters required for statistical model calculations are the strength functions, the average radiative widths, and the level densities. Systematic trends of

these quantities as a function of $(A + 1)$ are key ingredients to describing neutron-induced nuclear reactions with an optical model potential. In practice, coupling between levels, parameters of the potential, and the nucleus deformation parameter

TABLE VIII. ^{127}I and ^{129}I average capture cross section processed with the NJOY code at 293.6 K. Quoted uncertainties result from the statistical and systematic errors added quadratically.

Energy group (keV)	$^{127}\text{I}(n, \gamma)$ (b)	$^{129}\text{I}(n, \gamma)$ (b)
5.5–9.1	1.36 ± 0.05	0.85 ± 0.04
9.1–15.0	1.05 ± 0.04	0.65 ± 0.03
15.0–24.8	0.82 ± 0.03	0.50 ± 0.03
24.8–40.9	0.65 ± 0.03	0.37 ± 0.02
40.9–67.4	0.51 ± 0.02	0.26 ± 0.01
67.4–111.1	0.35 ± 0.01	0.18 ± 0.01

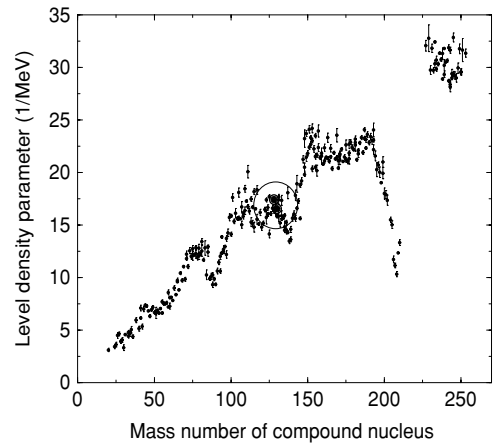


FIG. 12. Variation of the level density parameter a (Fermi gas model) with compound nucleus mass number. Our results (circle), deduced from the resonance shape analysis of the ^{127}I and ^{129}I data, are compared with the recommended data available in the RIPL-2 library.

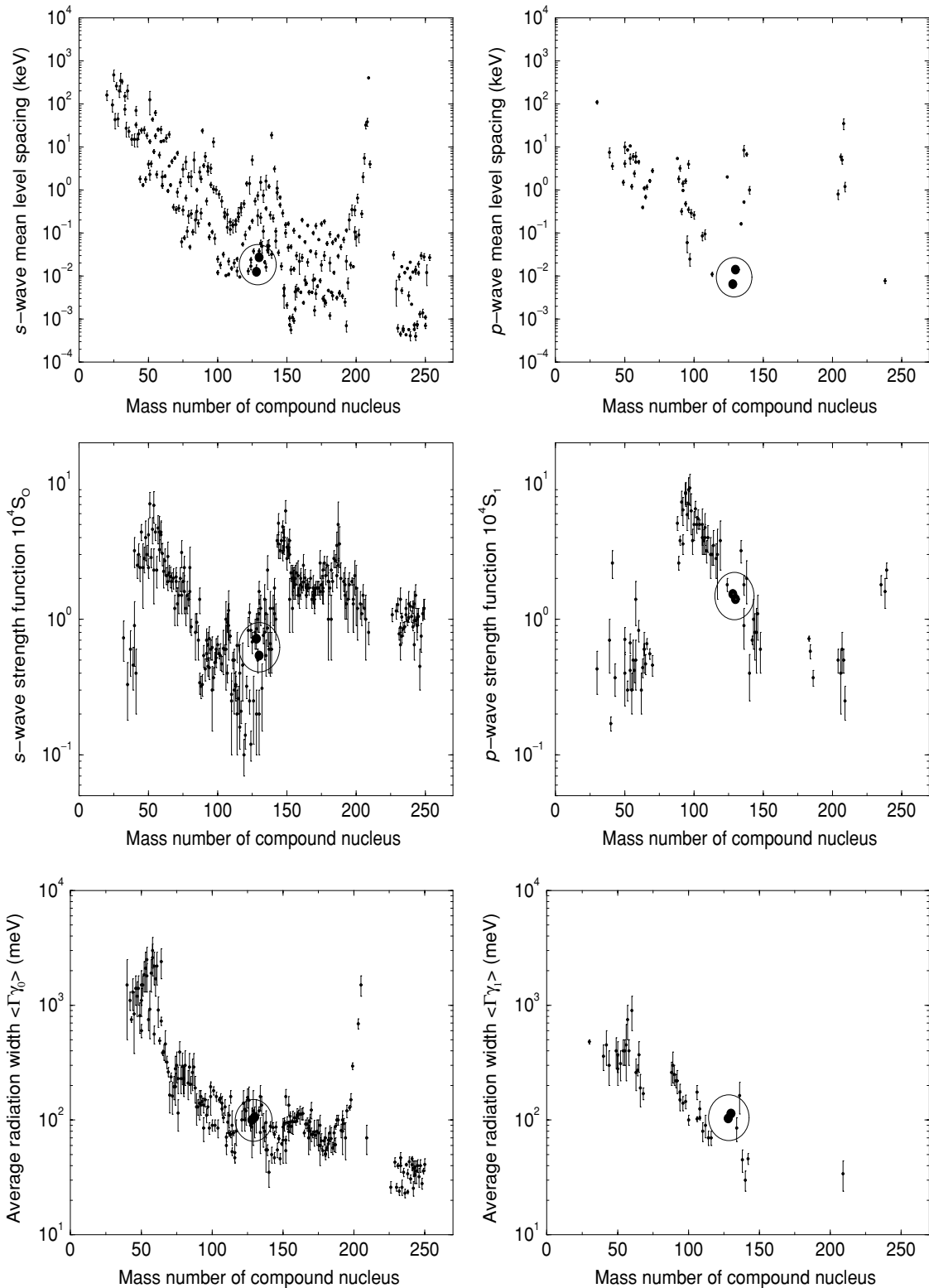


FIG. 13. Systematic trends of the mean level spacing, neutron strength function, and average radiation width with respect to the compound nucleus mass number. *s*- and *p*-wave parameters are shown separately. ^{127}I and ^{129}I average resonance parameters obtained in this work (circle) are compared with those available in the RIPL-2 library.

are fine tuned together with a few statistical model parameters in order to improve the consistency between optical model calculations and experimental data.

Statistical model parameters for theoretical calculations are compiled in the Reference Input Parameter Library RIPL-2. Figure 12 compares the level density parameters a obtained

in this work with those available in RIPL-2. Variations of $D_{l=1,2}$, $S_{l=1,2}$, and $(\Gamma\gamma_{l=1,2})$ with $A + 1$ are shown in Fig. 13. The neutron strength functions and average radiation widths determined in this work (Table VII) are consistent with the systematic trends followed by the RIPL data. For p waves, no recommended data are available around mass numbers 128 and 130.

For the mean level spacings, the comparison of our results with the RIPL data reveals huge discrepancies. Reliable level density parameters (or spin cutoff) are of great importance for any applications of the statistical theory. In the RIPL library, the recommended level densities around mass numbers 128 and 130 are, respectively, equal to 16.4 ± 0.3 and 15.9 ± 0.2 MeV^{-1} . These values are 6.2% and 4.1% lower than our ^{127}I and ^{129}I results (Table VI). The corresponding D_0 (D_1) parameters should be close to 22.6 eV (11.7 eV) for ^{127}I and 39.9 eV (20.6 eV) for ^{129}I . These l -dependent mean level spacings are systematically higher than our results. In typical optical model applications, these discrepancies have significant consequences on the calculation of the photon strength function and on the result of the Hauser-Feshbach GDR-based capture model.

The present results confirm the difficulty in determining confident s -wave mean level spacing and realistic fermion gas level density parameters from resonance shape analysis. Because of the experimental resolution of the facility, information on the resonance parameters is often incomplete. The final experimental D_0 value depends on (1) the number of observed resonances, (2) our capability to identify multiplets of resonances, (3) the model applied to distinguish s - and p -wave resonances, and (4) the method used to account for missing levels. In this work, we used the ESTIMA method which distinguishes s - and p -wave resonances according to their neutron width values in association with the properties of the Porter-Thomas distribution. This approach gives reliable results which have to be improved in the frame of the random matrix theory by using the properties of the Gaussian orthogonal ensemble and other involved statistical tests [54].

VI. CONCLUSION

^{127}I and ^{129}I capture and total cross sections have been measured and analyzed within the 0.5 eV to 100 keV neutron energy range. Below 10 keV, resonances have been interpreted individually in terms of Reich-Moore parameters. Assignments of the orbital momentum were performed with the ESTIMA method, relying on the Bayes theorem and on the properties of the Porter-Thomas reduced neutron width distribution. The analysis of the unresolved resonance range has been performed with the Hauser-Feshbach formula with width fluctuations. Consistent sets of statistical model parameters were obtained and successfully compared with those extracted from the resolved resonance range. For ^{127}I (^{129}I), the s -wave neutron strength function is close to 0.7×10^{-4} (0.5×10^{-4}), the effective potential scattering radius is 5.5 (5.7) fm, and the s -wave mean level spacing is 12.5 (27.3) eV. For the average radiation widths, we found ^{127}I (^{129}I) values ranging from 100.0 to 112.4 (106.0 to 114.2) meV. These results are fully consistent with the standard deviation of the distributions of

the $\Gamma\gamma$ values, which are 22.4 meV for ^{127}I and 15.2 meV for ^{129}I . The present results were used to improve the ^{127}I and ^{129}I evaluations in the latest version of the European library JEFF-3.1. For the description of the high-energy cross sections, coupled-channel optical model calculations were optimized with the statistical model parameters determined in this work.

The inspection of the s -wave mean level spacings with respect to the mass number of the compound nucleus has shown the difficulty in extracting consistent statistical model parameters from conventional time-of-flight data. A deeper investigation of the experimental limits of the spectrometer and more sophisticated statistical treatments of the resolved resonance parameters are needed to improve the accuracy of the average parameters. Next, studies have to focus on the advantages of the random matrix theory in association with conventional statistical tests and optical model calculations.

ACKNOWLEDGMENTS

The authors wish to express their appreciation for the work of C. Ingelbrecht and his sample preparation staff. Special thanks to the IRMM Linac operators for providing the neutron beam for the TOF measurements. We also express our gratitude to N. M. Larson and M. Moxon for their valuable discussions and relevant advice. The authors also thank F. Gunsing and T. Belgys for help in correcting this work. This work has been partly supported by the European Commission through Contract FIKW-CT-2000-00107 (n_TOF-ND-ADS Project).

APPENDIX: THE GILBERT AND CAMERON LEVEL DENSITY FORMULA

This Appendix presents the formula applied in this work to determine the fermion gas level density parameter and the p -wave mean level spacing for the $n + ^{127}\text{I}$ and $n + ^{129}\text{I}$ nuclear systems.

The study of the spacing between the neutron resonances sharing the same l in an interval ΔE containing N resonances provides a direct way of determining D_l :

$$D_l = \frac{\Delta E}{N}. \quad (\text{A1})$$

Alternatively, one may define the observed level density ρ_l as the number of levels per unit of energy:

$$\rho_l = \frac{1}{D_l}. \quad (\text{A2})$$

However, many sources of error may alter the level spacing deduced from neutron resonance data. Capture and transmission measurements are not precise enough to make sure that all resonances have been detected. Therefore, a semiempirical formula was introduced to predict reliable estimates of the level density ρ_J of all levels with spin J , regardless of parity (+ or -). It was developed on the basis of the Bethe free gas model, which considers the nucleus as being a Fermi gas of free nucleons confined to the nuclear volume. Gilbert and Cameron proposed a formula to account for the dependence of the various parameters on the mass number A , the odd-even

effect, the shell structure, and the nuclear deformation [32]. For iodine, the formula may be written as

$$\rho_J(E^*) = \frac{1}{3} \frac{a \exp \sqrt{4aE^*}}{\sigma(4aE^*)^{5/4}} \left[\exp \left(-\frac{J^2}{2\sigma^2} \right) - \exp \left(-\frac{(J+1)^2}{2\sigma^2} \right) \right], \quad (\text{A3})$$

in which E^* is the excitation energy, a represents the fermion gas level density parameter, and σ stands for a spin-dependent parameter often called the spin cutoff. The spin cutoff parameter is calculated as

$$\sigma^2 \simeq 0.1459 \sqrt{aE^*} (A+1)^{2/3}. \quad (\text{A4})$$

In the analysis of neutron resonances, the relevant parameter is the observed level density ρ_l rather than ρ_J which involves

both parities. Assuming equal probability for both parities, ρ_l may be defined as

$$\rho_l(E^*) = \frac{1}{2} \sum_J \rho_J(E^*). \quad (\text{A5})$$

For s -wave neutron resonances and a target nucleus with a ground state spin I and parity π , the states of the compound nucleus exhibit a spin either of $J = I + 1/2$ or $J = |I - 1/2|$ and a parity π . The level density of s -wave resonance is, therefore,

$$\rho_{l=0}(E^*) = \frac{1}{2} (\rho_{J=|I-1/2|}(E^*) + \rho_{J=I+1/2}(E^*)). \quad (\text{A6})$$

The fermion gas level density parameter for the compound nucleus ^{128}I and ^{130}I can be obtained from the experimental D_0 value by combining expressions (A3) and (A6). The p -wave mean level spacing is then calculated with Eq. (A5).

-
- [1] R. L. Macklin, Nucl. Sci. Eng. **85**, 350 (1983).
 [2] G. Noguere, A. Brusegan, A. Lepretre, N. Hault, R. Galleano, and E. Macavero, Nucl. Sci. Tech. Suppl. **2**, 184 (2002).
 [3] G. Noguere, A. Brusegan, A. Lepretre, N. Hault, O. Bouland, and G. Rudolf, in *Proceedings of the International Conference on Nuclear Data for Science and Technology*, Santa Fe, NM, 2004, edited by R. C. Haight, M. B. Chadwick, T. Kawano, and P. Talou (AIP, New York, 2005), p. 1462.
 [4] C. Ingelbrecht, J. Lupo, K. Raptis, T. Altitzoglou, and G. Noguere, Nucl. Instrum. Methods Phys. Res. A **480**, 204 (2002).
 [5] F. Gunsing, A. Lepretre, C. Mounier, C. Raepsaet, A. Brusegan, and E. Macavero, Phys. Rev. C **61**, 054608 (2000).
 [6] G. Noguere, CEA/DEN Cadarache Report No. CEA-R-6071, 2005.
 [7] F. Corvi, G. Fioni, F. Gasperini, and P. B. Smith, Nucl. Sci. Eng. **102**, 272 (1991).
 [8] C. Bastian, in *Proceedings of the International Conference on Neutrons in Research and Industry, Crète, Grèce, 1996*, edited by George Vourvopoulos (Society of Photo-optical Instrumentation Engineers, Bellingham, WA, 1997), p. 611.
 [9] F. H. Froehner, SESH computer code, General Atomic Report No. GA-8380, 1968.
 [10] T. A. Brody, J. Flores, J. B. French, P. A. Mello, A. Pandey, and S. S. M. Wong, Rev. Mod. Phys. **53**, 385 (1981).
 [11] C. E. Porter and R. G. Thomas, Phys. Rev. **104**, 483 (1956).
 [12] G. Breit and E. Wigner, Phys. Rev. **49**, 519 (1936).
 [13] M. C. Moxon and J. B. Brisland, REFIT computer code, Harwell Laboratory Report No. CBNM/ST/90-131/1, 1990.
 [14] N. M. Larson, SAMMY-M6 computer code, Oak Ridge National Laboratory Report No. ORNL/TM-9179/R6, 2003.
 [15] C. W. Reich and M. S. Moore, Phys. Rev. **111**, 929 (1958).
 [16] W. E. Lamb, Phys. Rev. **55**, 190 (1939).
 [17] C. Coceva and R. Magnani, IRMM Report No. GE/R/ND/96, 1996.
 [18] A. Brusegan, G. Noguere, and F. Gunsing, Nucl. Sci. Tech. Suppl. **2**, 685 (2002).
 [19] F. H. Froehner and O. Bouland, Nucl. Sci. Eng. **137**, 70 (2001).
 [20] J. R. Dunning, G. B. Pegram, G. A. Fink, and D. P. Mitchell, Phys. Rev. **48**, 265 (1935).
 [21] C. S. Wu, L. J. Rainwater, and W. W. Havens, Phys. Rev. **71**, 174 (1947).
 [22] L. Seren, H. N. Friedlander, and S. H. Turkel, Phys. Rev. **72**, 888 (1947).
 [23] H. Pomerance, Phys. Rev. **83**, 641 (1951).
 [24] B. Grimeland, Phys. Rev. **86**, 937 (1952).
 [25] R. B. Tattersall, H. Rose, S. R. Pattenden, and D. Jowitt, J. Nucl. Energy, Part A, Reactor Sci. **12**, 32 (1960).
 [26] J. W. Meadows and J. F. Whalen, Nucl. Sci. Eng. **9**, 132 (1961).
 [27] E. Jozefowicz, Nucleonics **8**, 437 (1963).
 [28] J. C. Robertson, Nucl. Phys. **71**, 417 (1965).
 [29] T. B. Ryves, J. Nucl. Phys. Energy **24**, 35 (1970).
 [30] L. Friedmann and D. C. Aumann, Radiochimica Acta **33**, 182 (1983).
 [31] T. Katoh, S. Nakamura, H. Harada, and Y. Ogata, Nucl. Sci. Tech. **36**, 223 (1999).
 [32] T. Belgya, G. L. Molnar, Z. Revay, and J. L. Weil, in *Proceedings of the International Conference on Nuclear Data for Science and Technology*, Santa Fe, NM, 2004, edited by R. C. Haight, M. B. Chadwick, T. Kawano, and P. Talou (AIP, New York, 2005), p. 744.
 [33] R. C. Block, G. G. Slaughter, and J. A. Harvey, Nucl. Sci. Eng. **8**, 112 (1960).
 [34] N. J. Pattenden, Nucl. Sci. Eng. **17**, 371 (1963).
 [35] J. Roy and D. Wuschke, Can. J. Chem. **36**, 1424 (1958).
 [36] S. Nakamura, H. Harada, T. Katoh, and Y. Ogata, Nucl. Sci. Tech. **33**, 283 (1996).
 [37] D. D. Wilkey and J. E. Willard, J. Chem. Phys. **44**, 970 (1966).
 [38] G. Noguere, Nuclear Energy Agency JEF Document No. JEF/DOC-986, 2005.
 [39] V. P. Alfimenkov, S. B. Borzakov, Vo Van Thuan, Yu. D. Mareev, L. B. Pikelner, A. S. Khrykin, and E. I. Sharapov, Nucl. Phys. **A398**, 93 (1983).
 [40] Y. Matsuda *et al.*, Phys. Rev. C **64**, 015501 (2001).
 [41] E. Fort and J. P. Doat, ESTIMA computer code, NEA Nuclear Data Committee Report No. NEANDC-161U, 1983.
 [42] L. M. Bollinger and G. E. Thomas, Phys. Rev. **171**, 1293 (1968).
 [43] S. Y. Oh, J. Chang, and L. C. Leal, Nucl. Sci. Eng. **148**, 43 (2004).
 [44] J-Ch. Sublet, P. Ribon, and M. Coste, CALENDF computer code, CEA/DEN Cadarache Report No. CEA-R-6020, 2003.
 [45] A. Gilbert and A. G. W. Cameron, Can. J. Phys. **43**, 1446 (1953).
 [46] J. B. Garg, J. Rainwater, and W. W. Havens, Phys. Rev. **137**, B547 (1965).

- [47] G. Rohr, R. Shelley, and A. Brusegan, in *Proceedings of the International Conference on Interactions of Neutrons with Nuclei*, Lowell, Massachusetts 1976, edited by E. Sheldon (National Technical Information Service, Springfield, 1976), p. 1249.
- [48] S. F. Mughabghab, M. Divadeenam, and N. E. Holden, *Neutron Cross Sections: Neutron Resonance Parameters and Thermal Cross Sections* (Academic, New York, 1981).
- [49] F. H. Frohner, *Nucl. Sci. Eng.* **103**, 119 (1989).
- [50] P. A. Moldauer, *Phys. Rev. C* **11**, 426 (1975).
- [51] P. A. Moldauer, *Nucl. Phys.* **A344**, 185 (1980).
- [52] W. Hauser and H. Feshbach, *Phys. Rev.* **87**, 366 (1952).
- [53] G. R. Satchler, *Phys. Lett.* **7**, 55 (1963).
- [54] A. Courcelle, in *Proceedings of the Workshop on the Future of Theory- and Experiment-Based Nuclear Data Evaluation*, Commissariat à l'Énergie Atomique, Bruyère-le-Châtel, September 26–28, 2005 (unpublished).